

1 **Investigation of the summer 2018 European ozone air pollution episodes using**
2 **novel satellite data and modelling**

3 Richard J. Pope^{1,2}, Brian J. Kerridge^{3,4}, Martyn P. Chipperfield^{1,2}, Richard Siddans^{3,4}, Barry G. Latter^{3,4},
4 Lucy J. Ventress^{3,4}, Matilda A. Pimlott¹, Wuhu Feng^{1,5}, Edward Comyn-Platt⁶, Garry D. Hayman⁷,
5 Stephen R. Arnold¹ and Ailish M. Graham¹

6
7 *1: School of Earth and Environment, University of Leeds, Leeds, United Kingdom*

8
9 *2: National Centre for Earth Observation, University of Leeds, Leeds, United Kingdom*

10
11 *3: Remote Sensing Group, STFC Rutherford Appleton Laboratory, Chilton, United Kingdom*

12
13 *4: National Centre for Earth Observation, STFC Rutherford Appleton Laboratory, Chilton, United*
14 *Kingdom*

15
16 *5: National Centre for Atmospheric Science, University of Leeds, Leeds, United Kingdom*

17
18 *6: European Centre for Medium-Range Weather Forecasts, Reading, UK*

19
20 *7: Centre for Ecology and Hydrology, Wallingford, United Kingdom*
21

22 Submitted to *Atmospheric Chemistry and Physics*

23 Correspondence to: Richard J. Pope (r.j.pope@leeds.ac.uk)

24 **Abstract:**

25 In the summer of 2018, Europe experienced an intense heat wave which coincided with several
26 persistent large-scale ozone (O₃) pollution episodes. Novel satellite data of lower tropospheric
27 column O₃ from the Global Ozone Monitoring Experiment-2 (GOME-2) and Infrared Atmospheric
28 Sounding Interferometer (IASI) on the MetOp satellite showed substantial enhancements in 2018
29 relative to other years since 2012. Surface observations also showed ozone enhancements across
30 large regions of continental Europe in summer 2018 compared to 2017. Enhancements to surface
31 temperature and the O₃ precursor gases carbon monoxide and methanol in 2018 were co-retrieved
32 from MetOp observations by the same scheme. This analysis was supported by the TOMCAT
33 chemistry transport model (CTM) to investigate processes driving the observed O₃ enhancements.
34 Through several targeted sensitivity experiments we show that meteorological processes, and
35 emissions to a secondary order, were important for controlling the elevated O₃ concentrations at the
36 surface. However, mid-tropospheric (~500 hPa) O₃ enhancements were dominated by
37 meteorological processes. We find that contributions from stratospheric O₃ intrusions ranged
38 between 15 - 40%. Analysis of back trajectories indicates that the import of O₃-enriched air masses
39 into Europe originated over the North Atlantic substantially increasing O₃ in the 500 hPa layer during
40 summer 2018.

43 1. Introduction

44 Over the past two decades there have been several intense summer-time heatwaves over Europe
45 (e.g. 2003 over continental Europe (Scott et al., 2004), 2006 over north-western Europe (Rebetz et
46 al., 2008) and 2010 across eastern Europe and Russia (Matsueda et al., 2011)). With current and
47 future climate change, increasing average global surface temperature is expected to trigger more
48 frequent and intense heatwaves (Lhotka et al., 2017; Guerreiro et al., 2018). The summer-time 2018
49 heatwave across predominantly north-western and central Europe and Scandinavia generated
50 temperature anomalies of approximately 2.0-4.0 K (Li et al., 2020; Drouard et al., 2020). Dynamically,
51 it was caused by a combination of intense anticyclonic blocking systems, Rossby wave dynamics and
52 the positive phase of the summer-time North Atlantic Oscillation (NAO+) (Li et al., 2020; Liu et al.,
53 2020; Drouard et al., 2020). Environmentally, the summer 2018 heatwave caused severe drought
54 conditions with decreased precipitation and soil moisture content (Bastos et al., 2020; Dirmeyer et
55 al., 2020), while negatively impacting natural vegetation (e.g. decreased gross primary productivity
56 (Smith et al., 2020; Bastos et al., 2020)). From a human health perspective, the 2018 heatwave
57 caused 863 temperature related excess deaths in the UK (PHE, 2019).

58 As well as meteorological and vegetation responses, enhancements in atmospheric pollutants from
59 heatwaves can lead to a degradation in air quality (AQ) across Europe. Blocking systems (anticyclonic
60 conditions) have been shown to increase the level of air pollutions such as carbon monoxide (CO;
61 Thomas and Devasthale, 2014), nitrogen dioxide (NO₂; Pope et al., 2014) and particulate matter (i.e.
62 PM_{2.5}; Graham et al., 2020) to hazardous levels. Pope et al., (2016) focused on the 2006 UK
63 heatwave and detected enhancements in surface O₃ through the accumulation of pollutants (i.e.
64 atmospheric blocking) but also the higher temperatures yielding more active atmospheric chemistry
65 (i.e. ozone formation). Papanastasiou et al., (2015) found that Greek heatwave conditions (2001-
66 2010) typically yielded an increase in NO₂, PM_{2.5} and O₃ by 14-29%, 25-38% and 12%, respectively.
67 Rasilla et al., (2019) found that heatwaves in Madrid only moderately increased NO₂ and O₃ but
68 significantly increased PM₁₀ concentrations. However, they associated this with enhanced long-
69 range transport of African dust and then accumulation under heatwave conditions. García-Herrera et
70 al., (2010) provided a review of the 2003 European heatwave finding that the Alpine region had
71 substantially elevated surface ozone levels (peaking at 417 µg/m³ with 68% of sites from 23
72 countries reaching concentrations above 180 µg/m³) when compared with the previous 12 summers.
73 Biogenic volatile organic compound (BVOC) emissions from vegetation are known to increase under
74 drought conditions from temperature stress (e.g. in the 2003 European heatwave; Rennenberg et
75 al., 2006). Churkina et al., (2017) found that heatwave conditions (2006) in Berlin yielded an increase
76 in BVOC emissions which contributed up to 12% of the surface ozone formation. Heatwaves can also
77 trigger wildfires, which emit primary air pollutions and can form secondary gases such as surface
78 ozone on a regional and hemispheric scale (Honrath et al., 2004). Overall, elevated surface O₃ is
79 associated with adverse health impacts (Doherty et al., 2017; Heal et al., 2013; Jerrett et al., 2009)
80 with ailments such as asthma, reduced lung function and disease (WHO, 2021). It also has adverse
81 impacts on the natural biosphere (Sitch et al., 2007) and agriculture (Hollaway et al., 2012; van
82 Dingenen et al., 2009), in turn reducing deposition of surface ozone on vegetation. In this study, we
83 use surface and satellite observations of O₃, in combination with the well-evaluated TOMCAT global
84 chemical transport model (CTM), to investigate the impact of the summer 2018 heatwave on
85 European AQ and determine the key processes driving observed surface/tropospheric O₃

86 enhancements. We describe the observations and model we have used in Section 2. Section 3 and
87 Section 4 discusses our results and discussion/conclusions, respectively.

88 **2. Observations and Model**

89 **2.1. Satellite and Surface Observations**

90 We use satellite observations of lower tropospheric O₃ (i.e. sub-column O₃ (SCO₃) between the
91 surface and 450 hPa) from the Global Ozone Monitoring Experiment (GOME-2) and the Infrared
92 Atmospheric Sounding Interferometer (IASI) instruments on-board ESA's MetOp-A satellite, which
93 was launched in 2006 into a sun-synchronous polar orbit with equator crossing times of 9:30 (day)
94 and 21:30 (night). GOME-2 is a nadir-viewing spectrometer with spectral coverage in the ultraviolet-
95 visible (UV-Vis) of 240–790 nm (Riese et al., 2012) and a ground footprint of 40 km × 80 km in the
96 first part of the mission and 40 km x 40 km from 2013 (once Metop-B was commissioned). IASI is a
97 Michelson interferometer which observes the infrared spectral range 645 to 2760 cm⁻¹ with spectral
98 sampling of 0.25 cm⁻¹ (Illingworth et al., 2011). It measures simultaneously in four fields of view
99 (circular at nadir with a diameter of 12 km) which are scanned across track to sample a 2200 km-
100 wide swath (Clerbaux et al., 2009).

101 For GOME-2, the Rutherford Appleton Laboratory (RAL) scheme uses an optimal estimation
102 algorithm (Rodgers, 2000) to retrieve height-resolved ozone distributions spanning the stratosphere
103 and troposphere (Miles et al., 2015). The scheme applied to GOME-2 has been developed from that
104 used first for GOME-1 on-board ERS-2 (Munro et al., 1998; Forster et al., 2007). This is a multi-step
105 scheme in which profile information is first retrieved in the stratosphere by exploiting wavelength-
106 dependent absorption in the O₃ Hartley band (270-307nm) and is then extended into the
107 troposphere by exploiting temperature-dependent spectral structure in the O₃ Huggins bands (325-
108 335nm). For IASI, O₃ profiles are retrieved using an extended version of RAL's Infrared-Microwave-
109 Sounding (IMS) scheme, which is described in Pope et al., (2021), Palmer et al., (2022) and Pimlott et
110 al., (2022). The IMS core scheme was originally developed to retrieve temperature, water vapour
111 and stratospheric O₃ profiles along with surface spectral emissivity and cloud jointly from co-located
112 measurements by IASI, the Microwave Humidity Sounder (MHS) and the Advanced Microwave
113 Sounding Unit (AMSU-A) on MetOp (RAL Space, 2015). GOME-2 and IMS O₃ data were filtered for a
114 geometric cloud fraction less than 0.2, a solar zenith angle less than 80°, a cost function less than
115 200.0 and a convergence flag equal to 1.0. Examples of the vertical sensitivity to retrieving ozone
116 (i.e. averaging kernels) from GOME-2 and IMS are shown in **Supplementary Material (SM) 1**.

117 We also use surface O₃ observations from the European Monitoring and Evaluation Programme
118 (EMEP) network for May-August 2017 and 2018. The EMEP network contains >100 surface
119 measurement sites measuring information on a range of air pollutions (e.g. ozone, NO₂ and PM_{2.5}).
120 EMEP surface data can be used for multiple scientific applications such as trends analysis (Yan et al.,
121 2018) and atmospheric chemistry model evaluation (Schultz et al., 2017; Archibald et al., 2020) and
122 is hosted by the EBAS database infrastructure, developed by the Norwegian Institute for Air
123 Research. In total, we used 125 spatial collocated EMEP sites in both years across Europe. Here, data
124 at individual sites were selected where the corresponding data flag was set to 0.0.

125 **2.2. Modelling & Sensitivity Experiments**

126 In this study the TOMCAT CTM (Chipperfield, 2006) is forced by European Centre for Medium-Range
127 Weather Forecasts (ECMWF) ERA-Interim reanalysis meteorology (Dee et al., 2011) and is run at a

128 horizontal resolution of $2.8^\circ \times 2.8^\circ$. The model has with 31 vertical levels from the surface to 10 hPa
129 with 5-7 (approximately 10) levels in the boundary layer (mid-troposphere), depending on latitude.
130 The model includes detailed tropospheric chemistry, including 229 gas-phase reactions and 82
131 advected tracers (Monks et al., 2017), and heterogeneous chemistry driven by size-resolved aerosol
132 from the GLOMAP module (Mann et al., 2010). Anthropogenic emissions used in this study come
133 from MACCity (Granier et al., 2011). The original dataset in Granier et al., (2011) derived emissions
134 up to 2010. Therefore, the Representative Concentration Pathways 8.5 (RCP 8.5) were used by
135 Granier et al., (2011) to generate emissions for later years (e.g. 2017 and 2018 as used in this study).
136 Fire emissions are from the Global Fire Assimilation System (GFAS, Kaiser et al., 2012) for 2017 and
137 2018. Year-specific off-line biogenic volatile organic compounds (VOCs) emissions for acetone,
138 methanol, isoprene and monoterpenes were simulated by the Joint UK Land Environment Simulator
139 (JULES – Pacifico et al., 2011; Best et al., 2011; Clark et al., 2011). All other biogenic VOC emissions
140 are climatological values and provided by the Chemistry-Climate Model Initiative (CCMI)
141 (Morgenstern et al., 2017). The global budgets of the JULES VOC emissions are low in comparison to
142 the climatological CCMI emissions, so were scaled up on a regional basis, while retaining the 2017-
143 2018 step change related to the 2018 summer heat wave. The full details of JULES VOC emissions
144 scaling can be found in **SM4**. Lightning emissions of NO_x are coupled to convection in the model,
145 which is derived from the meteorological reanalyses. Therefore, they vary in space and time
146 according to the seasonality and spatial pattern of convective activity (Stockwell et al., 1999). The
147 model was run for 2017 and 2018 with output at 6-hourly intervals (i.e. 00, 06, 12 and 18 UTC). Here,
148 each year was run with its respective meteorology and emissions and given the labels
149 Met17_Emis17 (representing 2017) and Met18_Emis18 (representing 2018).

150 To explore the importance of emission and meteorological processes behind the elevated European
151 summer 2018 tropospheric O_3 levels, a 1-year model sensitivity experiment was performed using
152 2018 meteorology but 2017 emissions (i.e. Met18_Emis17). Therefore, the difference between
153 Met18_Emis17 and Met17_Emis17 highlights the impact of fixed emissions (i.e. 2017 emissions for
154 both years), while the Met18_Emis18 minus Met18_Emis17 highlights the impact of fixed
155 meteorology (i.e. 2018 meteorology for both years – including BVOC emissions). These are
156 compared with the control differences for 2018-2017 (Met18_Emis18- Met17_Emis17). From here
157 on in, we refer to the control differences, fixed emission differences and the fixed meteorology
158 differences as CTL_DIFF, FIXED_EMIS_DIFF and FIXED_MET_DIFF, respectively. TOMCAT also
159 includes a stratospheric O_3 tracer, a common approach to tag stratospheric O_3 (e.g. Roelofs et al.,
160 2003; Akritidis et al., 2019), which can be used to investigate the impact of stratospheric O_3 intrusion
161 into the troposphere. The tracer is set equal to the model-calculated O_3 in the stratosphere. The only
162 tropospheric source of O_{35} is transport from the stratosphere while its sinks are via photolysis,
163 reactions with HO_2 , OH and H_2O through $\text{O}(^1\text{D})$ produced from O_{35} and surface deposition (Monks et
164 al., 2017). The tracer does not have a fixed lifetime but the loss rate in the troposphere depends on
165 the modelled local OH, HO_2 , H_2O and photolysis. Any O_3 that gets into the stratosphere will be
166 labelled as stratospheric before it returns. This was used to investigate the impact of stratospheric
167 O_3 intrusion into the troposphere.

168 TOMCAT has been used in a number of previous studies to investigate air quality and tropospheric
169 composition (e.g. Richards et al., 2013; Emmons et al., 2015; Pope et al., 2018; Pope et al., 2020)
170 whose results give confidence in the model's ability to simulate European tropospheric O_3 in this
171 study. Overall, when compared with observations, TOMCAT has good spatial agreement with both

172 GOME-2 and IASI and can reasonably reproduce the 2018 SCO₃ enhancement in 2018 versus 2017
173 (**SM 5**). The model also has good agreement, both in magnitude and seasonality, with the EMEP
174 observed surface concentrations (**SM 5**).

175 **2.3 ROTRAJ Back-trajectories**

176 We use the Reading Offline Trajectory Model (ROTRAJ) to generate air mass back-trajectories
177 (Methven et al., 2003) to assess the import of tropospheric O₃ into Europe. ROTRAJ is a Lagrangian
178 atmospheric transport model driven by meteorology from the same ECMWF ERA-Interim reanalyses
179 (horizontal resolution of 1.0125°) as used by TOMCAT. Velocity fields at the Lagrangian particle
180 positions are determined by cubic Lagrange interpolation in the vertical, bilinear interpolation in the
181 horizontal and linear interpolation in time. This method accounts for large scale advection since the
182 winds are resolved but does not resolve small scale sub-grid turbulent transport. Kinematic back-
183 trajectories were released at 6-hourly intervals (i.e. at 00, 06, 12 and 18 UTC) from Paris and Berlin,
184 both central locations over Europe in the region of summer-time 2018 O₃ enhancements, between
185 the 1st May and 31st August for both 2017 and 2018. The trajectories were released at the surface
186 and at approximately 500 hPa and integrated for 10 days with 6-hourly output (i.e. 41 trajectory
187 points including the starting location) to investigate the origin of air masses arriving in these altitude
188 regions of enhanced summer-time O₃ in 2018. In total, ROTRAJ was therefore run 8 times (2 years ×
189 2 altitudes × 2 locations).

190 To quantify the import of tropospheric O₃ into Europe, for each trajectory, all the trajectory points
191 were co-located with corresponding TOMCAT O₃ mixing ratio values (i.e. the horizontal and vertical
192 grid box the trajectory point sits within and corresponding time stamp) and then the average O₃-
193 weighted back-trajectory (O₃-WBT) determined (i.e. back-trajectories with larger O₃WBT values
194 come from air masses with larger O₃ content). This follows a similar approach to Graham et al.,
195 (2020) and Stirling et al., (2020), though using a model chemical tracer and not emission inventories.

196 **3. Results**

197 **3.1 Surface Temperature**

198 Several studies (e.g. Li et al., 2020; Liu et al., 2020; Drouard et al., 2020) have documented the
199 intense heat wave across Europe in the summer of 2018. This is further shown in **Figure 1** which
200 compares surface temperature, co-retrieved with ozone and other variables from MetOp-A by the
201 IMS scheme, between 2017 and 2018. In May, higher temperatures occur across Scandinavia (5.0-
202 10.0 K), eastern Europe (3.0-7.0 K) and the UK (1.0-3.0 K), but temperatures are lower (-3.0 to -1.0 K)
203 across Iberia. In June, a similar spatial distribution occurs but the magnitude of the differences is
204 smaller. In July the largest temperature increases range from 6.0-8.0 K in Scandinavia to 2.0-6.0 K in
205 the UK/France. Iberia continued to experience temperatures lower by -2.0 to 0.0 K. In August, there
206 are near-zero differences over the UK, Iberia and most of Scandinavia but with increases of 1.0-3.0 K
207 over eastern Europe and Finland.

208 **3.2 Satellite Ozone**

209 We investigate the longer-term variability in tropospheric O₃ (i.e. SCO₃) to determine if 2017 is a
210 suitable comparator for the 2018 summer O₃ enhancements as it is for temperature. **Figure 2** shows
211 the 2012-18 SCO₃ average between May and August for a domain over the Atlantic and Europe and
212 the difference for the same season between specific years and the 2012-18 average. In 2012 and
213 2013, there are significant positive differences from the average between 1.0 DU and 5.0 DU over

214 much of the domain. Over continental Europe, the differences are smaller. Here, the significance of
215 differences between the year-specific and long-term averages are determined using the Wilcoxon
216 Rank test (Pirovano et al., 2012) at the 95% confidence level. In 2014 and 2015, there are negative
217 differences across Europe (-4.0 DU to -1.0 DU). In 2016, similar negative differences are primarily
218 across the north and south-east of the domain. In 2017, there are near-zero differences across the
219 Atlantic, UK and western Europe. Over eastern Europe and Mediterranean, there are significant
220 negative differences of between -2.0 DU and -1.0 DU. In 2018, across continental Europe there are
221 significant positive differences between 2.0 DU and 4.0 DU. As the 2017 differences are relatively
222 small in magnitude with a low proportion of significant pixels (i.e. Sig Pixels % = 32.7 is the lowest
223 across the 7 years), it is representative of average conditions for comparison with 2018. For 2018,
224 the summer SCO₃ enhancements across continental Europe are the largest for the years shown with
225 a coherent cluster of significant differences. This illustrates that the summer 2018 SCO₃
226 enhancements are a substantial deviation from the average conditions (which we represent as 2017
227 hereon) and that this is an intense O₃ event.

228 Investigation of SCO₃ retrieved from both GOME-2 (**Figure 3**) and the IMS scheme (**Figure 4**) show
229 consistent enhancements in summer 2018. In 2017, between May and August, GOME-2 typically
230 observed SCO₃ values between 20.0-30.0 DU across continental Europe. Peak SCO₃ values occurred
231 over the Mediterranean (30.0-38.0 DU); relatively high ozone is a typical feature of the
232 Mediterranean in summer (Richards et al., 2013). In 2018, the seasonality is consistent with 2017,
233 but the continental European SCO₃ values ranged between 25.0 DU and 35.0 DU. For the 2018-2017
234 difference, SCO₃ enhancements occur across continental Europe in all four months but peaked in
235 May and July between 3.0 DU and 8.0 DU, while typically 1.0-5.0 DU in June and August. The spatial
236 distribution of IMS-retrieved SCO₃ is similar to that of GOME-2 in 2017 and 2018, although the
237 absolute values tend to be systematically lower by 3.0-4.0 DU. However, despite this systematic
238 offset, the 2018-2017 differences are reasonably consistent with GOME-2. Across continental
239 Europe, IMS SCO₃ shows 2018 enhancements in all months investigated, but peaks in May and July,
240 like GOME-2, between 3.0 DU and 6.0 DU. The differences range from 1.0 DU to 3.0 DU in June and
241 are approximately 1.0 DU in August (though a peak enhancement of 3.0-5.0 DU occurs over the
242 Mediterranean). Spatial correlations between the GOME-2 and IASI difference (i.e. 2018-2017) maps
243 for the months investigated ranged between 0.21 and 0.47 (see **SM 5**).

244 The GOME-2 and IASI instruments observe UV-Vis and IR wavelengths, with peak vertical sensitivities
245 to tropospheric O₃ in the lower and mid/upper troposphere, respectively. Consistency in the 2018
246 enhancements in SCO₃ indicates that these extend over the bulk of the troposphere and increases
247 confidence in the detected enhancements for both sensors.

248 Investigation of several satellite-retrieved O₃ precursor gases (see **SM 2**) showed enhancements in
249 total column methanol (TCCH₃OH, **Figure S2**), especially linked to May and July temperature
250 enhancements (**Figure 1**), minor increases in tropospheric column NO₂ (TCNO₂, **Figure S3**) in May and
251 July over central Europe and widespread enhancements (weakest in July and strongest in August) in
252 total column carbon monoxide (TCCO, **Figure S4**). Investigation of the GOME-2 and IASI total column
253 O₃ (TCO₃) differences between 2017 and 2018 (**Figures S5 & S6**) showed these to be in close
254 agreement. Some spatial structure is similar to that of the SCO₃ difference patterns (**Figures 3 and**
255 **4**), with correlations of approximately 0.5 between TCO₃ and SCO₃ for each instrument (see **SM 3**).
256 Given the complex relationship between tropospheric O₃, precursor gases, atmospheric chemistry
257 (e.g. NO_x or VOC-limited regimes), surface deposition and meteorological conditions (e.g.

258 atmospheric temperatures and transport), a detailed chemistry transport model is required to assess
259 the key processes leading to the observed SCO₃ enhancements over Europe.

260 3.3 Surface Ozone

261 Increased temperatures during heat waves have been shown to enhance surface O₃ concentrations
262 (e.g. Jacob and Daniel, 2009; Vieno et al., 2010; Pyrgou et al., 2018). In the summer (May-June-July-
263 August, MJJA) of 2018, EMEP recorded larger O₃ mixing ratios across most of Europe in comparisons
264 to 2017 (**Figure 5a & b**). Over central Europe, surface O₃ mixing ratios ranged from approximately
265 45.0 ppbv to over 60.0 ppbv, while in 2017 it was 35.0 ppbv to 50.0 ppbv. Over the UK and north-
266 western Europe, surface O₃ mixing ratios ranged from 20.0 ppbv to 30.0 ppbv and then 25.0 ppbv to
267 35.0 ppbv in MJJA 2017 and 2018, respectively. In Scandinavia and eastern Europe, surface O₃ mixing
268 ratios ranged from 20.0 ppbv to 35.0 ppbv in MJJA 2017, while increasing to 25.0 ppbv to
269 approximately 40.0 ppbv in MJJA 2018. **Figure 5c** highlights these widespread enhancements where
270 domain-average surface O₃ mixing ratios are larger by typically 5.0-10.0 ppbv in May and from mid-
271 June to mid-August in 2018. **Figure 5d** shows that the domain median surface O₃ concentration
272 across MJJA was larger by 2.0-3.0 ppbv in 2018, but the 2018 extremes were greater with 75th and
273 95th percentiles of 45.0 ppbv and 55.0 ppbv in 2017 and 48.0 ppbv and 59.0 ppbv in 2018. Therefore,
274 surface observations of O₃ recorded widespread enhancements in MJJA 2018 compared to 2017
275 with peak site differences >10.0 ppbv. This is generally consistent with the 2018 layer-averaged
276 enhancements in the satellite-retrieved SCO₃ for regions where both datasets have spatial coverage.

277 3.4. Model Simulations

278 We use the TOMCAT model to investigate different factors potentially driving the observed
279 enhancements in tropospheric O₃. In comparisons with the observations (see **SM 5**) the model
280 reproduces the sign and spatial distribution of observed 2018-2017 differences reasonably well.
281 Although it has a tendency to underestimate the absolute magnitude, we are confident in the
282 model's ability to simulate the tropospheric O₃ enhancements relative to 2017.

283 At the surface (**Figure 6**), TOMCAT CTL_DIFF (i.e. Met18_Emis18 - Met17_Emis17) suggests that O₃ is
284 enhanced in May over Scandinavia (2.0- >5.0 ppbv), north-western Europe (0.0-2.0 ppbv), the Arctic
285 Ocean (>5.0 ppbv) and off the coast of Iberia (3.0-5.0 ppbv). However, negative values exist over
286 eastern Europe (-3.0 ppbv to -1.0 ppb) and the Atlantic west of Ireland (-3.0 ppbv to -1.0 ppb). In
287 June, the negative differences persist in eastern Europe (-3.0 ppbv to -1.0 ppb), but positive
288 differences are located over northern Scandinavia (1.0-2.0 ppbv) and the North Atlantic (2.0-4.0
289 ppbv). For July, CTL_DIFF shows the largest enhancements over continental Europe (i.e. Po Valley,
290 France, Benelux region and Iberia) and the UK (>5.0 ppbv). Negative differences of between -3.0
291 ppbv and -1.0 ppbv remain over eastern Europe. In August, the only clear differences are over Iberia
292 and the western Mediterranean, ranging between 3.0 ppbv and >5.0 ppbv. Overall, TOMCAT
293 simulates sub-regional surface O₃ enhancements over Europe, which are generally consistent with
294 EMEP observations apart from several sites over eastern Europe.

295 At 500 hPa, TOMCAT CTL_DIFF shows larger-scale O₃ enhancements in 2018 compared to 2017 (>5.0
296 ppbv) throughout May to August. In May and August, there are, however, a few negative differences
297 (-5.0 ppbv to -3.0 ppbv) over far eastern Europe. In June and July, the full domain is more or less
298 dominated by O₃ enhancements in 2018. In **Figures 3** and **4** (and **SM 5**), GOME-2 and IASI (and
299 TOMCAT with the instrument averaging kernels (AKs) applied to account for the vertical sensitivity of

300 the retrievals, see **SM 5** for more information) show SCO_3 enhancements during these months of
301 2018. Given the vertical extents and peak heights of their retrieval sensitivities and consistency in
302 spatial patterns (**Figs SM 9 and 11**) it is evident that the O_3 enhancements detected by GOME-2 and
303 IASI extend over the free troposphere. The model shows large-scale O_3 enhancements in the free
304 troposphere and similar patterns to GOME-2 and IASI when averaging kernels applied. So, the model
305 corroborates this finding from the satellite retrievals. Signals from EMEP and TOMCAT at the surface,
306 on the other hand, are more mixed across the domain.

307 The right-hand column of **Figure 6** shows the relative difference in the stratospheric O_3 contribution
308 to the 500 hPa O_3 layer (i.e. Strat % @ 500 hPa), from CTL_DIFF, between 2017 and 2018. Here, the
309 percentage of stratospheric O_3 contributing to the O_3 concentration at the 500 hPa is calculated for
310 2017 and 2018 and then the 2018-2017 difference determined. The largest enhancement to the 500
311 hPa layer was in July where the stratospheric O_3 contribution increased by 3.0% to >5.0% across
312 Europe. In June and August, the spatial patterns are similar with stratospheric O_3 contribution
313 enhancements of 3.0-5.0% across southern Europe, Scandinavia and the North Atlantic (above the
314 UK). In the North Atlantic, UK and northern Europe, there are near-zero changes in June and August.
315 In May, there are enhancements >5.0% across the northern region of the domain and northern
316 Africa, while smaller enhancements (1.0%-3.0%) over the UK and near-zero changes over eastern
317 Europe. This is partially supported by analysis of TCO_3 (see **SM 3**) where there are reasonable spatial
318 correlations (~0.5 to 0.6) between the SCO_3 2017-2018 summer differences and the equivalent for
319 TCO_3 . Therefore, these results indicate a potentially enhanced contribution of stratospheric O_3 into
320 the mid-troposphere during the summer of 2018 across Europe.

321 To quantify the separate importance of precursor emissions and meteorology in governing the
322 summer 2018 O_3 enhancements we compare the sensitivity experiments with the control runs.
323 **Figure 7** (left column) shows the results for the fixed emissions differences (i.e. FIXED_EMIS_DIFF)
324 between years (i.e. Met18_Emis17 – Met17_Emis17). At the surface, the FIXED_EMIS_DIFF show
325 similar spatial patterns to that of CTL_DIFF (**Figure 6** – left column). The domain spatial difference
326 correlations between these simulations is greater than 0.96 for all months considered. However,
327 FIXED_EMIS_DIFF (**Figure 7** - left column) tends to be lower than CTL_DIFF (**Figure 6** – left column)
328 by approximately 0.0-2.9 ppbv (i.e. positive red regions are weaker and negative blue regions
329 stronger in intensity). Therefore, the Met18_Emis17 run struggles to reproduce the absolute surface
330 O_3 enhancements in the Met18_Emis18 run. When the fixed meteorology differences
331 (FIXED_MET_DIFF, i.e. Met18_Emis18 - Met18_Emis17, **Figure 8** - left column) are compared with
332 CTL_DIFF, the surface 2018-2017 differences are substantially different.

333 Surface FIXED_MET_DIFF ranges between 0.0 ppbv and 2.0 ppbv across the domain in May and June
334 and is more confined to continental Europe in July and August. This shows that TOMCAT simulates
335 lower 2018 summer-time O_3 when 2017 emissions are used and indicates that emissions do have
336 some role in controlling O_3 levels at the surface. However, as the spatial difference pattern for
337 FIXED_MET_DIFF (**Figure 8** – left column) is different to that of CTL_DIFF (**Figure 6** – left column),
338 spatial correlations between them range from -0.53 to 0.54 over the four months, it suggests that
339 meteorology is important in governing the spatial distribution of CTL_DIFF. This is supported by the
340 fact that FIXED_MET_DIFF - CTL_DIFF (**Figure 8** left column – **Figure 6** left column) yields absolute
341 domain variations between 0.0 ppbv and 12.2 ppbv. Therefore, the two sensitivity experiments
342 suggest meteorology and emissions both play important roles in controlling surface O_3 during the

343 summer of 2018, but meteorology predominantly governs the spatial pattern and absolute
344 magnitude of the O₃ enhancements.

345 At 500 hPa, comparison of FIXED_EMIS_DIFF and CTL_DIFF show very consistent spatial patterns
346 across the four months with correlations all above 0.98. In terms of the absolute differences
347 between FIXED_EMIS_DIFF and CTL_DIFF (i.e. **Figure 7** centre column – **Figure 6** centre column) it
348 peaks at approximately 2.8 ppbv. For FIXED_MET_DIFF, the spatial correlation with CTL_DIFF, as for
349 the surface, is variable with values between -0.38 and 0.43. The absolute differences between
350 FIXED_MET_DIFF and CTL_DIFF (i.e. **Figure 8** centre column – **Figure 6** centre column) ranges from
351 0.0 ppbv to 14.8 ppbv. Therefore, emissions have a secondary role in controlling the O₃ while
352 meteorology is by far the dominant factor. For Strat % @ 500 hPa, the spatial correlations between
353 CTL_DIFF and FIXED_EMIS_DIFF are above 0.95 for all months and the absolute differences between
354 them (i.e. **Figure 7** right column - **Figure 6** right column) are near-zero. Comparison of
355 FIXED_MET_DIFF and TC_CTL shows spatial difference correlations ranging between -0.33 and 0.71
356 and absolute differences (i.e. **Figure 8** right column - **Figure 6** right column) peaking at 12.9%.
357 Therefore, as expected, meteorological processes are dominating the influence of the stratospheric
358 O₃ contribution (i.e. through stratosphere-troposphere exchanges) to the 500 hPa layer during the
359 summer 2018 O₃ enhancements over Europe.

360 To investigate the importance of stratospheric-troposphere exchange to the middle troposphere
361 enhancement (i.e. as shown in the TOMCAT 500 hPa layer and the satellite SCO₃ data), **Figures 9** and
362 **10** show TOMCAT control run zonal 2018-2017 difference cross-sections (for the domain longitudes)
363 of O₃ profiles and the stratospheric O₃ contribution to each pressure layer. In May and June, in the
364 lower troposphere (approximately surface to 800 hPa), there are negative (-3.0% to 0.0%) and
365 positive (0.0% to 3.0%) differences between 30-50°N and 50-70°N, respectively. During June, there
366 are positive differences (0.0% to 5.0%) across most latitudes and in August, the opposite occurs to
367 that of May/June. In the mid-troposphere (800-300 hPa), positive differences occur in most months
368 (0.0-5.0% in May, 0.0-7.0% in June, >10% in July and 5.0-10.0% in August), though in May and August
369 negative differences (-5.0% to 0.0%) exist around 40°N and 55°N. This is consistent with the 500 hPa
370 O₃ differences in **Figure 6** (centre panels). In the upper troposphere – lower stratosphere (UTLS,
371 approximately 300-100 hPa) there are limbs of positive O₃ differences (i.e. >10%, 5.0-10.0 ppbv)
372 propagating into the mid-troposphere (30-40°N in May, 30-50°N in June, 40-50°N in July and 30-40°N
373 & 60-70°N in August), suggestive of stratospheric intrusion into the mid-troposphere. Using the
374 stratospheric O₃ tracer in TOMCAT, **Figure 10** shows the enhanced proportion of O₃ originating from
375 the stratosphere in the summer of 2018. Interestingly, for all months (apart from May between 30-
376 45°N), there are enhanced contributions of stratospheric O₃ (15.0% to >50.0%) in the lower-mid
377 troposphere (i.e. below 500 hPa). In absolute terms, this is only a minor contribution typically <1.0
378 ppbv below 800 hPa. Between 800-400 hPa, this increases to 1.0-5.0 ppbv (remains relatively
379 consistent in percentage terms) in most months and latitude bands. In the UTLS, it increases to 5.0-
380 10.0% enhancements in stratospheric O₃ contributions, which is consistent with its proximity to the
381 stratosphere. In comparison between **Figures 9** and **10**, where there are enhancements in the
382 stratospheric O₃ contribution but negative differences in O₃ (e.g. in June in the lower troposphere
383 between 50°N and 55°N) which is suggestive of different processes influencing the O₃ concentrations
384 (e.g. descent of relatively small stratospheric O₃ contributions but advection of tropospheric O₃ away
385 from the region). Overall though, in the mid-troposphere, where there are larger enhancements in
386 O₃, there are similar responses in the stratospheric O₃ contribution. For June, the mid-troposphere

387 O₃ enhancement is approximately 5.0-7.0 ppbv with a signal of 1.0-2.0 ppbv in the stratospheric
388 tracer. Therefore, in the more extreme cases, the stratospheric O₃ contribution is approximately
389 15.0-40.0% to the mid-tropospheric O₃ enhancements in summer 2018 over Europe. However, a
390 separate study would be required to undertake a detailed assessment of the meteorological
391 processes controlling the enhanced stratospheric intrusion of ozone in the summer of 2018 and how
392 it compares to other years (how does it compare with years other than 2017).

393 The two remaining factors, linked to meteorological processes (as suggested above), which may
394 affect the O₃ enhancements in 2018 are increased summer temperatures (e.g. through enhanced
395 kinetic rates), and the import of tropospheric O₃ from upwind (e.g. North America from the
396 prevailing winds). **Figure 11** shows the 2017-2018 zonal temperature differences (i.e. same as **Figure**
397 **9** but for temperature) with the correlation between the 2017 and 2018 temperature and O₃
398 differences overplotted. Qualitatively, the zonal differences in O₃ and temperature have some
399 similarities. There are positive differences (temperature differences of 0.0-1.0%) between 50-60°N at
400 the surface and 400 hPa in May and June. Then in July, collocated positive differences (peaking at
401 2.0% or 3.0 K) exist between 50-70°N from the surface to 300 hPa. In August, there is no clear
402 relationship between temperature and O₃ enhancements. In all months (to a lesser extent in
403 August), in the UTLS, there are spatial agreements with positive differences between approximately
404 30-45°N and negative differences between 50/55-70°N. In terms of correlations (i.e. temporal
405 correlation in each grid box using the TOMCAT 6-hourly time series), the spatial agreement is
406 relatively weak. In all months, most of domain has relatively small values ranging between -0.5 to
407 0.5. There are only a few locations with strong correlations (i.e. > 0.5), which are in the UTLS or in
408 the lower-mid troposphere between 50-70°N (June & August) and 45-55°N in July near the surface.
409 Overall, the relationship between increased temperatures and enhanced kinetic rates yielding more
410 ozone formation is non-linear, so it is unsurprising that the direct comparisons of temperature and
411 ozone 2018-2017 differences above shows no clear pattern. Therefore, future work could include a
412 further sensitivity experiment running TOMCAT for 2018, but with 2017 temperatures used in the
413 chemistry routines to quantify the role of temperature in the summer 2018 O₃ enhancements.

414 To investigate the potential advection of tropospheric O₃-rich air masses into Europe we have used
415 ROTRAJ back-trajectories to determine the O₃WBTs (i.e. an indicator of air mass O₃ content). As
416 shown in **SM 6**, there is large variability in the O₃WBT values and spatial distribution (i.e. **Figures S13**
417 **and 14**), so they have to be gridded onto the TOMCAT horizontal resolution (see **Figures S15 and 16**).
418 While this approach does not directly account for the frequency of trajectory points in each grid box,
419 **Figures S13 and S14** show there is widespread coverage across the North Atlantic. This results in
420 >500 trajectory points near the receptor sites (i.e. Paris and Berlin), ~100 trajectory points around
421 the edge of Europe and 25-50 trajectory points in the North Atlantic (not shown here). Overall, this
422 spatial distribution is relatively consistent and does not change substantially between years (typically
423 10%), thus this approach is suitable in this study. **Figure 12** shows the differences (2018-2017)
424 between the gridded O₃WBTs where the back-trajectories have been released at the surface from
425 Paris (**Figure 12a**), at the surface from Berlin (**Figure 12b**), at approximately 500 hPa from Paris
426 (**Figure 12c**) and at approximately 500 hPa from Berlin (**Figure 12d**). We selected Paris and Berlin as
427 they are situated in central Europe where the summer 2018 O₃ enhancements have been observed
428 while the surface and 500 hPa are the altitudes of primary focus in the modelling work.

429 At the surface, Paris and Berlin show consistent patterns. Over the North Atlantic (i.e. origin of the
430 prevailing winds into Europe), there are typically negative O₃WBT values between -5.0 ppbv and -1.0

431 ppbv suggesting that advection of O₃ into Europe during the summer (i.e. May-August) was
432 predominantly larger in 2017 and did not strongly contribute to the 2018 observed surface O₃
433 enhancements. Advection of O₃-rich air in 2018 did originate from Scandinavia into continental
434 Europe, though the number of trajectories is relatively low (see **Figure S13**). As both locations show
435 similar relationships, it provides confidence in this methodology. At 500 hPa, the 50-60°N spatial
436 pattern is less defined with values typically between -5.0 and 5.0 ppbv for both locations. However,
437 in the southern North Atlantic (30-50°N) there are positive differences of approximately 3.0-10.0
438 ppbv for both release locations. Note that as free-tropospheric winds tend to have larger horizontal
439 velocities, the back-trajectories generally start from further away closer to North America. Again,
440 given the broad similarity in differences between both release locations, it provides confidence in
441 this approach. Overall, our results indicate a larger transport of O₃ to the surface of continental
442 Europe in 2017, while at approximately 500 hPa the import of O₃ into Europe is larger in 2018. Here,
443 the positive differences originate from the southern North Atlantic (i.e. a larger range of locations,
444 absolute values and homogeneous signal than the mixed differences between 50-60°N).

445 One potentially important factor is dry deposition of O₃ to the land surface. Due to the heatwave,
446 stress on the biosphere and the associated die back of vegetation could potentially reduce the
447 efficiency of O₃ deposition decreasing the O₃ sink (i.e. O₃ is more likely to deposit onto land covered
448 by vegetation than bare soil). Investigation of the normalised difference vegetation index (NDVI),
449 from the IMS scheme, between the summers of 2017 and 2018 did not highlight any spatially
450 coherent changes (not shown here). As a result, there is no obvious large-scale spatial vegetation die
451 back in 2018 due to the heatwave and thus the impact this would have on ozone deposition in
452 TOMCAT. Therefore, we ran two further experiments where the bare soil fraction for each grid box
453 over Europe was increased and decreased by 25% in summer 2018. This was to investigate the
454 sensitivity of surface ozone deposition to changes in the land surface. For the increase in bare soil
455 fraction there was a moderate systematic increase in European summer ozone by 0.0-1.5 ppbv (i.e.
456 less ozone deposition). When the bare soil fraction was decreased by 25%, this yielded a small
457 decrease in surface ozone by approximately 0.5 ppbv. Overall, a sizable level of vegetation die back
458 would be required for decreased ozone dry deposition to substantially contribute to the summer
459 2018 surface ozone enhancements.

460 **4. Discussion and Conclusions**

461 The summer of 2018 produced an intense heatwave across most of Europe with a substantial impact
462 on tropospheric temperatures, droughts, stress on vegetation and human mortality. Observations of
463 surface temperature, precursor gases and total column O₃ (TCO₃) experienced enhancements in
464 2018 relative to 2017. In this paper, we have demonstrated a strong enhancement in surface and
465 tropospheric O₃ during the heatwave between May and August 2018. The EMEP surface data
466 suggest an average European enhancement, relative to 2017, peaking at approximately 10.0 ppbv in
467 July and August. Investigation of lower tropospheric O₃ (i.e. surface-450 hPa sub-column O₃ – SCO₃)
468 from the GOME-2 and IASI instruments also showed enhancements, peaking at 5.0-10.0 DU, relative
469 to 2017. Analysis of the long-term GOME-2 SCO₃ record indicates 2017 to be a suitably
470 neutral/average reference year and the enhancement in 2018 to be anomalously large. Our
471 comparisons were therefore made between the summers of 2017 and 2018.

472 Consistency between the UV (GOME-2) and IR (IASI) sounders was important to our analysis because
473 their vertical sensitivities peak in the lower and mid-upper troposphere, respectively. The similar

474 patterns of SCO₃ enhancement detected by the two sounders therefore indicate that these extend
475 over the bulk of the troposphere, supportive of surface/lower tropospheric ozone enhancements.
476 This consistency also provides confidence that the complementary vertical sensitivities of GOME-2
477 and IASI ozone retrievals could be exploited in further investigation of tropospheric ozone in the
478 future (e.g. long-term trends from multiple platforms/retrieval schemes have shown large-scale
479 inconsistencies in other studies e.g. Gaudel et al., (2018)).

480 Tropospheric O₃ behaviour is complex and the summer 2018 enhancements over Europe could
481 potentially have been caused by various factors: atmospheric chemistry, meteorology (e.g.
482 temperature, advection of O₃-rich air masses), anthropogenic and natural precursor emissions, dry
483 deposition and stratospheric intrusion. To investigate the interactions between these processes,
484 potentially leading to the summer 2018 O₃ enhancements, we used the well-evaluated TOMCAT 3D
485 CTM. Evaluation of the model in this study showed that it could accurately capture the spatial
486 pattern, temporal evolution and sign (i.e. positive 2018-2017 O₃ differences) of the O₃
487 enhancements and that, although it underestimated the observed enhancements, TOMCAT is an
488 adequate tool to investigate them.

489 The results of several model simulations showed that the surface ozone enhancements (mainly in
490 north-western Europe) in the summer of 2018 were predominantly driven by meteorological
491 processes with emissions acting as a secondary factor. As the ROTRAJ back-trajectories suggest that
492 advection of summer-time O₃ was larger in 2017, the 2018 European O₃ enhancements at surface
493 level were likely from in-situ processes. The TOMCAT stratospheric O₃ tracer indicated a negligible
494 contribution of stratospheric O₃ to these surface enhancements. At 500 hPa, the enhancement in
495 tropospheric O₃ is much larger spatially across Europe and dominated by meteorological processes.
496 Intrusion of stratospheric O₃ into the mid-troposphere has a moderate influence on the
497 observed/modelled O₃ enhancements with contributions of up to 15.0-40.0%. Correlations between
498 TOMCAT temperature and O₃ enhancements show broad agreement at some latitudes (e.g. 50-70°N
499 in the lower-mid troposphere). However, this relationship is non-linear and difficult to quantify
500 without further simulations/model tracers, which was beyond the scope of this study. ROTRAJ back-
501 trajectories suggest that in 2018, relative to 2017, there is the advection of more O₃-rich airmasses
502 into the European mid-troposphere contributing to the summer 2018 O₃ enhancements at this
503 altitude. Therefore, in the summer of 2018 over Europe, in-situ meteorological processes appear to
504 be predominantly driving surface O₃ enhancements over Europe, while advection of tropospheric O₃-
505 rich air and stratospheric intrusion are driving the corresponding tropospheric O₃ enhancements

506 Overall, through our study focusing on the European summer 2018 air pollution episode, we have
507 demonstrated the use of novel satellite datasets and a modelling framework (i.e. targeted sensitivity
508 experiments and model tracers) suitable to investigate the air quality impacts from future European
509 heatwaves such as that which occurred in summer 2022.

510 **Acknowledgements**

511 This work was funded by the UK Natural Environment Research Council (NERC) by providing funding
512 for the National Centre for Earth Observation (NCEO, award reference NE/R016518/1).

513 **Conflicting Interests**

514 The authors declare that they have no conflicts of interest.

515

516 **Date Availability**

517 The TOMCAT simulations are publicly available at
518 http://homepages.see.leeds.ac.uk/~earrjpo/european_summer_2018_o3/tomcat, while the RAL
519 Space satellite can be found at
520 http://homepages.see.leeds.ac.uk/~earrjpo/european_summer_2018_o3/satellite. The EMEP
521 surface O₃ data was obtained from <http://ebas-data.nilu.no/default.aspx>. The GOME-2 tropospheric
522 column NO₂ data was downloaded from EUMETSAT at https://acsaf.org/nrt_access.php. The
523 TOMCAT and RAL Space satellite data will be uploaded to the Zenodo open access portal
524 (<https://zenodo.org/>) if this manuscript is accepted for publication in ACP after the peer-review
525 process.

526 **Author Contributions**

527 RJP, MPC and BJK conceptualised and planned the research study. RJP performed the TOMCAT
528 model simulations with support from MPC and WF. The JULES BVOC emissions were provided by ECP
529 and GDH. RJP analysed the satellite data provided by RAL Space (BJK, RS, BGL and LJV) with support
530 from BJK, RS and BGL. RJP undertook the EMEP analysis. RJP ran ROTRAJ with technical support from
531 SRA and AMG. RJP prepared the manuscript with contributions from all co-authors.

532 **References**

- 533 Akritidis, D., Pozzer, A. and Zanis, P. 2019. On the impact of future climate change on tropopause
534 folds and tropospheric ozone. *Atmospheric Chemistry and Physics*, **19**, 14387–14401, doi:
535 10.5194/acp-19-14387-2019.
- 536 Archibald, A.T., et al. 2020. Description and evaluation of the UKCA stratosphere–troposphere
537 chemistry scheme (StratTrop vn 1.0) implemented in UKESM1. *Geoscientific Model Development*, **13**,
538 1223–1266, doi: 10.5194/gmd-13-1223-2020.
- 539 Bastos, A., Ciais, P., Friedlingstein, P., et al.: Direct and seasonal legacy effects of the 2018 heat wave
540 and drought on European ecosystem productivity, *Science Advances*, **6**, eaba2724,
541 doi:10.1126/sciadv.aba2724, 2020.
- 542 Best, M.J., Pryor, M., Clark, D.B., et al.: The Joint UK Land Environment Simulator (JULES), model
543 description—Part 1: energy and water fluxes, *Geoscientific Model Development*, **4**, 677–699,
544 doi:10.5194/gmd-4-677-2011, 2011.
- 545 Chipperfield, M.P.: New version of the TOMCAT/SLIMCAT off-line chemistry transport model:
546 Intercomparison of stratospheric trace experiments, *Quarterly Journal of the Royal Meteorological*
547 *Society*, **132**, 1179–1203, doi:10.1256/qj.05.51, 2006.
- 548 Churkina, G., Kuik, F., Bonn, B., et al. 2017. Effect of VOC Emissions from Vegetation on Air Quality in
549 Berlin during a Heatwave. *Environmental Science and Technology*, **51**(11), 6120–6130, doi:
550 10.1021/acs.est.6b06514.
- 551 Clark, D. B., Mercado, L.M., Sitch, S., et al.: The Joint UK Land Environment Simulator (JULES), model
552 description—Part 2: carbon fluxes and vegetation dynamics, *Geoscientific Model Development*, **4**,
553 701–722, doi:10.5194/gmd-4-701-2011, 2011.
- 554 Clerbaux, C., Boynard, A., Clarisse, L., et al.: Monitoring of atmospheric composition using the
555 thermal infrared IASI/MetOp sounder, *Atmospheric Chemistry and Physics*, **9** (16), 6041–6054,
556 doi:10.5194/acp-9-6041-2009, 2009.

557 Dee, D.P., Uppala, S.M., Simmons, A.J., et al.: The ERA-Interim reanalysis: Configuration and
558 performance of the data assimilation system, *Quarterly Journal of the Royal Meteorological Society*,
559 137 (656), 553–597, doi:10.1002/qj.828, 2011.

560 Dirmeyer, P.A., Balsamo, G., Blyth, E.M., et al.: Land-Atmosphere Interactions Exacerbated the
561 Drought and Heatwave Over Northern Europe During Summer 2018, *AGU Advances*, 2,
562 e2020AV000283., doi: 10.1029/2020AV000283, 2020.

563 Doherty, R. M., Heal, M. R., and O’Connor, F. M.: Climate change impacts on human health over
564 Europe through its effect on air quality, *Environmental Health*, 16(1), 33–44, doi:10.1186/s12940-
565 017-0325-2, 2017.

566 Drouard, M., Kornhuber, K. and Woollings, T.: Disentangling Dynamical Contributions to Summer
567 2018 Anomalous Weather Over Europe, *Geophysical Research Letter*, 46, 12537-12546,
568 doi:10.1029/2019GL084601, 2020.

569 Emmons, L. K., Arnold, S. R., Monks, S. A., et al.: The POLARCAT Model Intercomparison Project
570 (POLMIP): overview and evaluation with observations, *Atmospheric Chemistry and Physics*, 15, 6721–
571 6744, doi:10.5194/acp-15-6721-2015, 2015.

572 Forster, P., Ramaswamy, V., Artaxo, P., et al.: Changes in Atmospheric Constituents and in Radiative
573 Forcing, in: *Climate Change 2007: The Physical Science Basis. Contribution of Working Group I to the*
574 *Fourth Assessment Report of the Intergovernmental Panel on Climate Change*, Cambridge University
575 Press, Cambridge, United Kingdom and New York, NY, USA, 2007.

576 García-Herrera, R., Díaz, J., Trigo, R.M., et al. 2020. A Review of the European Summer Heat Wave of
577 2003. *Critical Reviews in Environmental Science and Technology*, 40(4), 267-
578 306, doi:10.1080/10643380802238137. Gaudel, A., Cooper, O.R., Ancellet, G., et al.: Tropospheric
579 Ozone Assessment Report: Present day distribution and trends of tropospheric ozone relevant to
580 climate and global atmospheric chemistry model evaluation. *Elementa*, 6(39), 1-58,
581 doi:10.1525/elementa.291, 2018.

582 Graham, A. M., Pringle, K. J., Pope, R. J., et al.: Impact of the 2019/2020 Australian megafires on air
583 quality and health, *GeoHealth*, 5, e2021GH000454, doi:10.1029/2021GH000454, 2020.

584 Granier, C., Bessagnet, B., Bond, T., et al.: Evolution of anthropogenic and biomass burning emissions
585 of air pollutants at global and regional scales during the 1980–2010 period, *Climatic Change*, 109,
586 163-190, doi:10.1007/s10584-011-0154-1, 2011.

587 Guerreiro, S.B., Dawson, R.J., Kilsby, C., et al.: Future heat-waves, droughts and floods in
588 European cities, *Environmental Research Letters*, 13, 034009, 10.1088/1748-9326, 2018.

589 Heal, M.R., Heaviside, C., Doherty, R.M., et al. 2013. Health burdens of surface ozone in the UK for a
590 range of future scenarios. *Environment International*, 61, 36-44, doi:10.1016/j.envint.2013.09.010.

591 Hollaway, M.J., Arnold, S.R., Challinor, A. J. and Emberson, L.D: Intercontinental trans-boundary
592 contributions to ozone-induced crop yield losses in the North Hemisphere, *Biogeosciences*, 9, 271–
593 2929, doi: 10.5194/bg-9-271-2012, 2012.

594 Honrath, R.E., Owen, R.C., Val Martin, M., et al. 2004. Regional and hemispheric impacts of
595 anthropogenic and biomass burning emissions on summertime CO and O₃ in the North Atlantic
596 lower free troposphere. *Journal of Geophysical Research: Atmospheres*, 109(D24), doi:
597 10.1029/2004JD005147.

598 Jacob, D.J., and Winner, D.A.: Effect of climate change on air quality, *Atmospheric Environment*, 43
599 (1), 51-63, doi:10.1016/j.atmosenv.2008.09.051, 2009.

600 Jerrett, M., Burnett, R.T., Pope, C.A., et al.: Long-term ozone exposure and mortality, *The New*
601 *England Journal of Medicine*, 360 (11), 1085–1095, doi: 10.1056/NEJMoa0803894, 2009.

602 Kaiser, J.W., Hell, A., Andreae, M.O., et al.: Biomass burning emissions estimated with a global fire
603 assimilation system based on observed fire radiative power, *Biogeosciences*, 9(1), 527–554, doi:
604 10.5194/bg-9-527-2012, 2012.

605 Lhotka, O., Kysely, J. and Farda, A.: Climate change scenarios of heat waves in Central Europe and
606 their uncertainties, *Theoretical and Applied Climatology*, 131, 1043-1054, doi: 10.1007/s00704-016-
607 2031-3, 2017.

608 Li, M., Yao, Y., Simmonds, I., et al.: Collaborative impact of the NAO and atmospheric blocking on
609 European heat waves, with a focus on the hot summer of 2018, *Environmental Research Letters*, 15,
610 114003, doi:10.1088/1748-9326/aba6ad, 2020.

611 Liu, X., He, B., Guo, L., et al.: Similarities and differences in the mechanisms causing the European
612 summer heat waves in 2003, 2010 and 2018, *Earth's Future*, e2019EF001386, doi:
613 10.1029/2019EF001386, 2020.

614 Mann, G.W., Carslaw, K.S., Spracklen, D.V., et al.: Description and evaluation of GLOMAP-mode: A
615 modal global aerosol microphysics model for the UKCA composition-climate model. *Geoscientific*
616 *Model Development*, 3(2), 519–551, doi:10.5194/gmd-3-519-2010, 2010.

617 Matsueda, M.: Predictability of Euro-Russian blocking in summer of 2010, *Geophysical Research*
618 *Letters*, 38, L06801, doi:10.1029/2010GL046557, 2011.

619 Methven, J., Arnold, S.R., O'Connor, F.M., et al.: Estimating photochemically produced ozone
620 throughout a domain using flight data and a Lagrangian model, *Journal of Geophysical Research:*
621 *Atmospheres*, 10 (D9), doi:10.1029/2002JD002955, 2003.

622 Miles, G.M., Siddans, R., Kerridge, B. J., Latter, B. G., and Richards, N. A. D.: Tropospheric ozone and
623 ozone profiles retrieved from GOME-2 and their validation, *Atmospheric Measurement Techniques*,
624 8, 385–398, doi:10.5194/amt-8-385-2015, 2015.

625 Monks, S.A., Arnold, S.R., Hollaway, M. J., et al.: The TOMCAT global chemistry transport model v1.6:
626 Description of chemical mechanism and model evaluation, *Geoscientific Model Development*, 10 (8),
627 3025–3057, doi:10.5194/gmd-10-3025-2017, 2017.

628 Morgenstern, O., Hegglin, M.I., Rozanov, E., et al.: Review of the global models used with phase 1 of
629 the Chemistry-Climate Model Initiative (CCMI), *Geoscientific Model Development*, 10 (2), 639–671,
630 doi:10.5194/gmd-10-639-2017, 2017.

631 Munro, R., Siddans, R., Reburn, W. J., and Kerridge, B. J.: Direct measurement of tropospheric ozone
632 distributions from space, *Nature*, 392, 168–171, doi:10.1038/32392, 1998.

633 Pacifico, F., Harrison, S.P., Jones, C.D., et al.: Evaluation of a photosynthesis-based biogenic isoprene
634 emission scheme in JULES and simulation of isoprene emissions under present-day climate
635 conditions, *Atmospheric Chemistry and Physics*, 11, 4371–4389, doi:10.5194/acp-11-4371-2011,
636 2011.

637 Palmer, P., I., Marvin, M., R., Siddans, R., et al.: Nocturnal survival of isoprene linked to formation
638 of upper tropospheric organic aerosol, *Science*, 375 (6580), 562-566,
639 doi:10.1126/science.abg4506.

640 Papanastasiou, D.K., Melas, D. and Kambezidis, H.D., 2015. Air quality and thermal comfort levels
641 under extreme hot weather. *Atmospheric Research*, 152, 4-13, doi:
642 10.1016/j.atmosres.2014.06.002.

643 PHE (Public Health England), PHE heatwave mortality monitoring, available at:
644 [https://assets.publishing.service.gov.uk/government/uploads/system/uploads/attachment_data/file](https://assets.publishing.service.gov.uk/government/uploads/system/uploads/attachment_data/file/942648/PHE_heatwave_report_2018.pdf)
645 [/942648/PHE_heatwave_report_2018.pdf](https://assets.publishing.service.gov.uk/government/uploads/system/uploads/attachment_data/file/942648/PHE_heatwave_report_2018.pdf) (last accessed 3rd February 2022), 2019.

646 Pimlott, M.A., Pope, R.P., Kerridge, B.J., et al.: Investigating the global OH radical distribution using
647 steady-state approximations and satellite data. *Atmospheric Chemistry and Physics*, **22**, 10467-
648 10488, doi: 10.5194/acp-22-10467-2022, 2022.

649 Pirovano, G., Balzarini, A., Bessagnet, B., et al.: Investigating impacts of chemistry and transport
650 model formulation on model performance at European scale, *Atmospheric Environment*, 53, 93–109,
651 doi:10.1016/j.atmosenv.2011.12.052, 2012.

652 Pope, R.J., Savage, N.H., Chipperfield, M.P., et al.: The influence of synoptic weather regimes on UK
653 air quality: analysis of satellite column NO₂, *Atmospheric Science Letters*, 15, 211– 217,
654 doi:10.1002/asl22.492, 2014.

655 Pope, R.J., Butt, E.W., Chipperfield, M.P., et al.: The impact of synoptic weather on UK surface ozone
656 and implications for premature mortality. *Environmental Research Letters*, **11**, 124004,
657 doi:10.1088/1748-9326/11/12/124004, 2016.

658 Pope, R.J., Chipperfield, M.P., Arnold., S.R., et al. 2018. Influence of the wintertime North Atlantic
659 Oscillation on European tropospheric composition: an observational and modelling study.
660 *Atmospheric Chemistry and Physics*, **18**, 8389–8408, doi: 10.5194/acp-18-8389-2018.

661 Pope, R.J., Arnold, S.R., Chipperfield, M.P., et al.: Substantial Increases in Eastern Amazon and
662 Cerrado Biomass Burning-Sourced Tropospheric Ozone. *Geophysical Research Letters*, 47 (3),
663 e2019GL084143, doi:10.1029/2019GL084143, 2020.

664 Pope, R. J., Kerridge, B. J., Siddans, R., et al.: Large enhancements in southern hemisphere satellite-
665 observed trace gases due to the 2019/2020 Australian wildfires, *Journal of Geophysical Research:*
666 *Atmospheres*, 1–13, doi:10.1029/2021jd034892, 2021.

667 Pyrgou, A., Hadjinicolaou, P and Santamouris, M: Enhanced near-surface ozone under heatwave
668 conditions in a Mediterranean island, *Scientific Reports*, 8, 9191, doi:10.1038/s41598-018-27590-z,
669 2018.

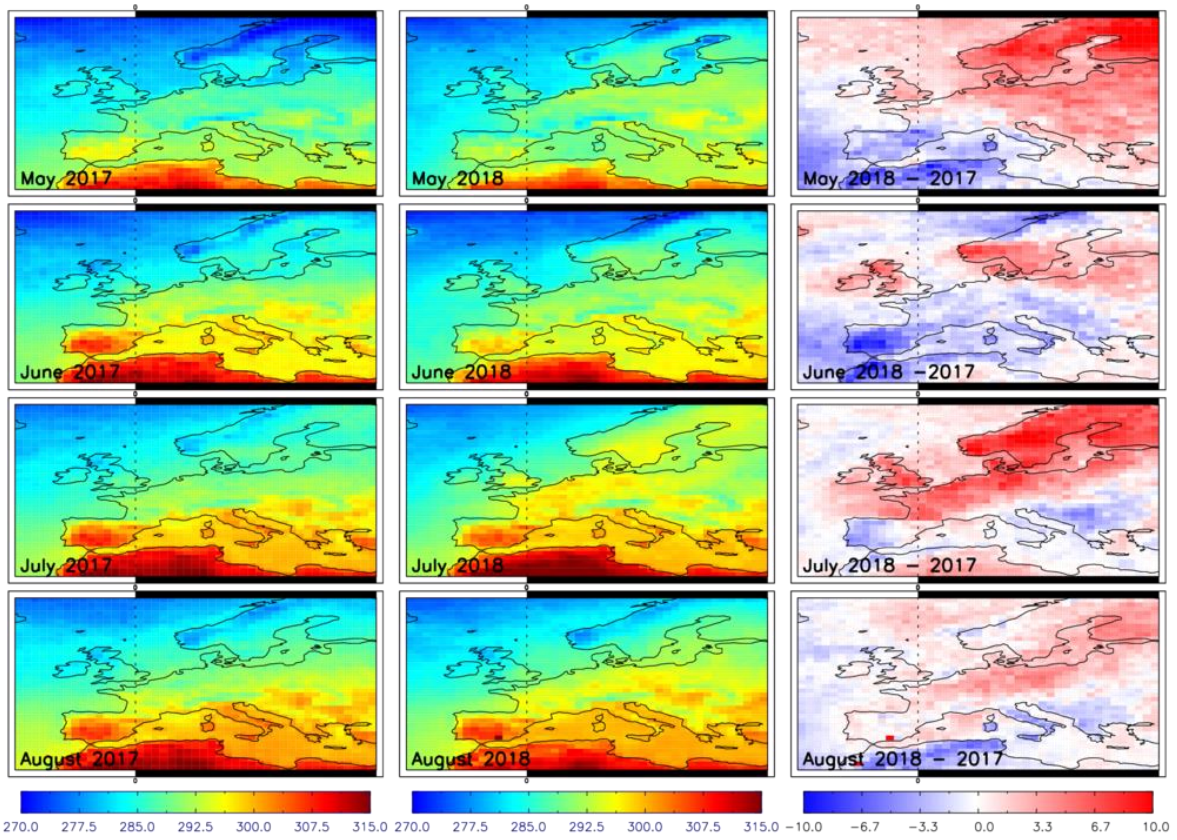
670 RAL Space, Optimal Estimation Method retrievals with IASI, AMSU and MHS – Final Report Version
671 5.2, available at: http://cedadocs.ceda.ac.uk/1377/1/iasi_mhs_final_report_v5p2.pdf (last accessed
672 17/08/2020), 2015.

673 Rasilla, D., Allende, F., Martilli, A., et al. 2019. Heat Waves and Human Well-Being in Madrid (Spain).
674 *Atmosphere*, 10(5), 288-309, doi: 10.3390/atmos10050288.

675 Rebetez, M., Dupont, O. and Giroud, M.: An analysis of July 2006 heatwave extent in Europe
676 compared to the record year of 2003, *Theoretical and Applied Climatology*, 95, 1-7,
677 doi:10.1007/s00704-007-0370-9, 2008.

- 678 Renneberg, H., Loreto, F., Polle, A., et al. 2006. Physiological Responses of Forest Trees to Heat and
679 Drought. *Plant Biology*, **8**(5), 556-571, doi: 10.1055/s-2006-924084.
- 680 Richards, N.A.D, Arnold, S.R., Chipperfield, M.P., et al.: The Mediterranean summertime ozone
681 maximum: global emission sensitivities and radiative impacts, *Atmospheric Chemistry and Physics*,
682 **13**, 2231-2345, doi:10.5194/acp-13-2331-2013, 2013.
- 683 Riese, M., Ploeger, F., Rap, A., et al.: Impacts of uncertainties in atmospheric mixing on simulated
684 UTLS composition and related radiative effects, *Journal of Geophysical Research: Atmospheres*, **117**,
685 D16305, doi:10.1029/2012jd017751, 2012.
- 686 Rodgers, C.D.: Inverse methods for atmospheric sounding: Theory and practice. New Jersey, USA:
687 World Science. 2000.
- 688 Roelofs, G.L., Kentarchos, A.S., Trickl, T., et al. 2003. Intercomparison of tropospheric ozone models:
689 Ozone transport in a complex tropopause folding event. *Journal of Geophysical Research*, **108** (D12),
690 8529, doi: 10.5194/acp-19-14387-2019.
- 691 Schultz, M.G., Schroder, S., Lyapina, O., et al. 2017. Tropospheric Ozone Assessment Report:
692 Database and metrics data of global surface ozone observations. *Elementa – Science of the*
693 *Anthropocene*, **5**(58), doi: 10.1525/elementa.244.
- 694 Scott, P.A., Stone, D.A. and Allen, M.R.: Human contributions to the European heatwave of 2003,
695 *Nature*, **432**, 610-614, doi:10.1038/nature03089, 2004.
- 696 Sitch, S., Cox, P.M., Collins, W.J., & Huntingford, C.: Indirect radiative forcing of climate change
697 through ozone effects on the land carbon sink, *Nature*, **448**, 791–795, doi:10.1038/nature06059,
698 2007.
- 699 Smith, N.E., Kooijmans, L.M.J., Koren, G., et al.: Spring enhancements and summer reduction in
700 carbon uptake during the 2018 drought in Northwestern Europe, *Philosophical Transactions B*, **375**,
701 20190509, doi:10.1098/rstb.2019.0509, 2020.
- 702 Stockwell, D., Giannakopoulos, C., Plantevin, P.-H., et al. 1999. Modelling NO_x from lightning and its
703 impact on global chemical fields. *Atmospheric Environment*, **33**, 4477–4493, doi: 10.1016/S1352-
704 2310(99)00190-9.
- 705 Thomas, M.A. and Devasthale, A.: Sensitivity of free tropospheric carbon monoxide to atmospheric
706 weather states and their persistency: an observational assessment over the Nordic countries,
707 *Atmospheric Chemistry and Physics*, **14**, 11545–11555, doi:10.5194/acp14-11545-2014, 2014.
- 708 Van Dingenen, R., Dentener, F.J., Raes, F., et al.: The global impact of ozone on agriculture crop
709 yields under current and future air quality legislation. *Atmospheric Environment*, **43**(3), 604–618,
710 doi:10.1016/j.atmosenv.2008.10.033, 2009.
- 711 Vieno, M., Dore, A.J., Stevenson, D.S., et al.: Modelling surface ozone during the 2003 heat-wave in
712 the UK, *Atmospheric Chemistry and Physics*, **10**, 7963–7978, doi:10.5194/acp-10-7963-2010, 2010.
- 713 WHO (World Health Organisation), Ambient (outdoor) air pollution, available at:
714 [https://www.who.int/news-room/fact-sheets/detail/ambient-\(outdoor\)-air-quality-and-health](https://www.who.int/news-room/fact-sheets/detail/ambient-(outdoor)-air-quality-and-health) (last
715 accessed 3rd February 2022), 2021.
- 716 Yan, Y., Pozzer, A., Ojha, N., et al. 2018. Analysis of European ozone trends in the period 1995—
717 2014. *Atmospheric Chemistry and Physics*, **18**(8), 5589—5605, doi: 10.5194/acp-18-5589-2018.

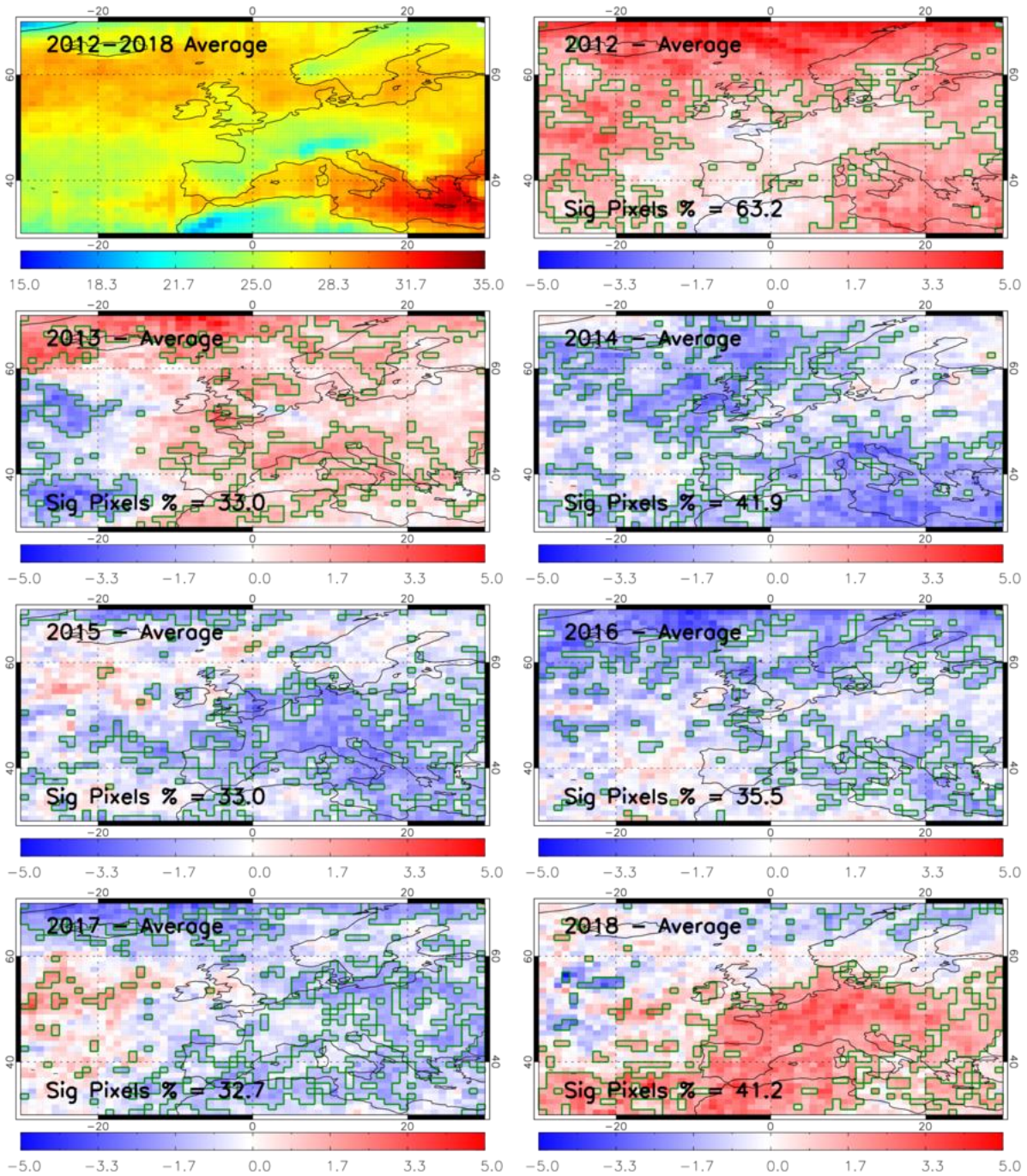
718 Figures:



719

720 **Figure 1:** Surface temperature (K) over Europe for May to August in 2017 (left column), 2018 (centre
721 column) and 2018-2017 difference (right column) retrieved from MetOp-A IASI, MHS and AMSU by
722 the IMS scheme.

723



724

725

726

727

728

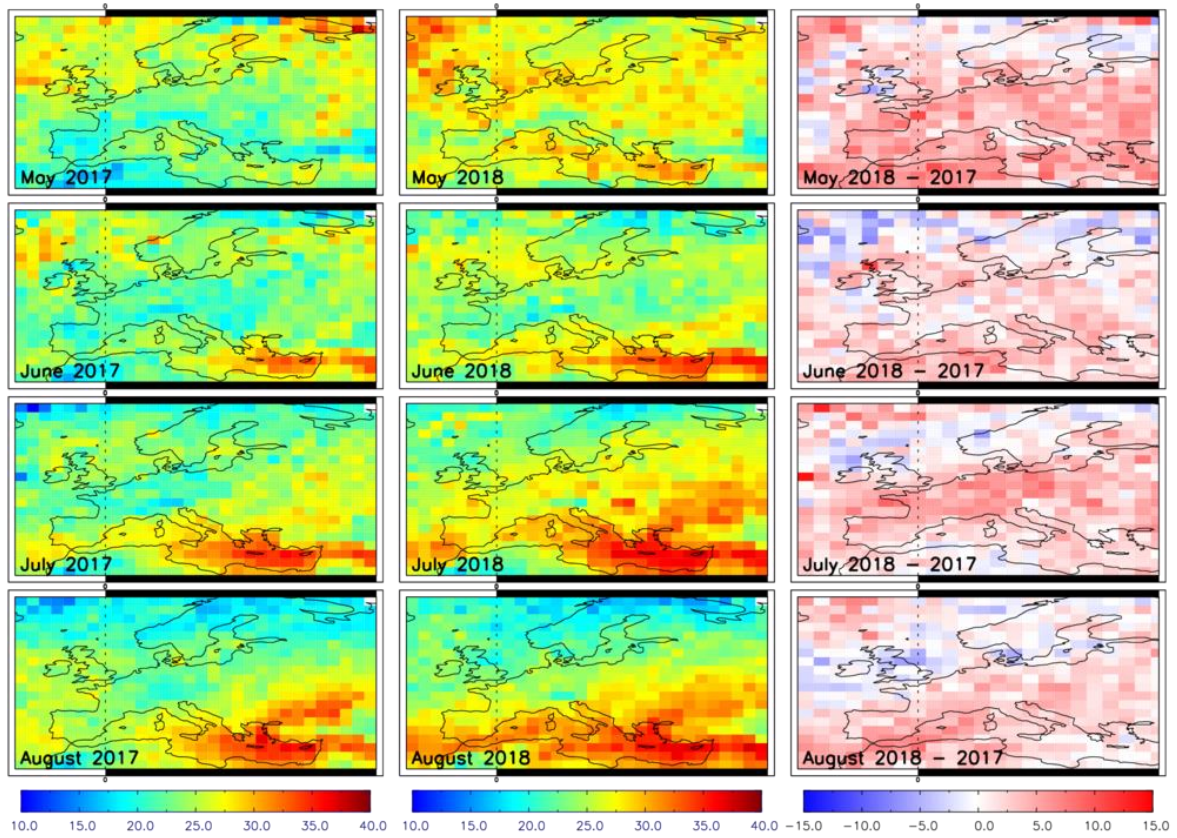
729

730

731

732

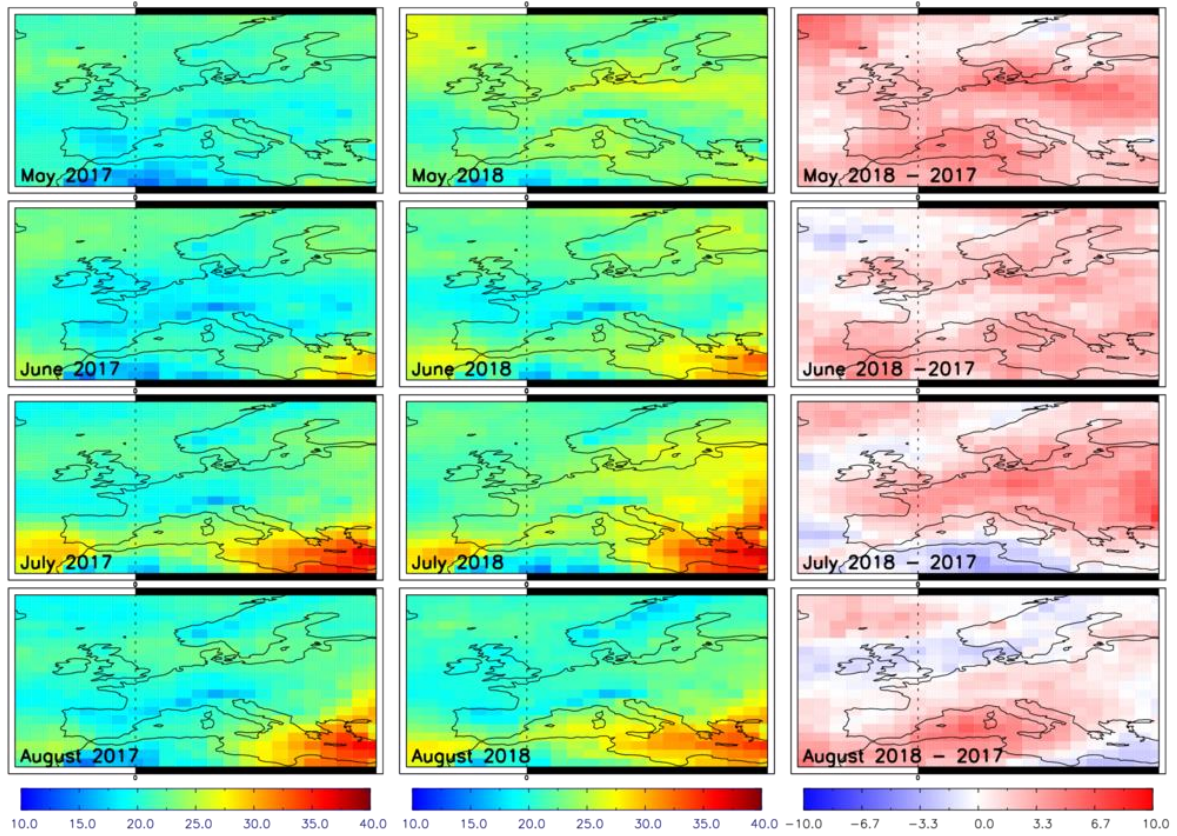
Figure 2: Sub-column ozone (SCO_3 , surface-450 hPa), in Dobson units (DU), retrieved from GOME-2 on Metop-A averaged across May to August between 2012 and 2018 (top left panel) and the corresponding difference from the 2012-18 mean for each year, respectively. The green-polygon-outlined regions show where the year-specific seasonal average is significantly different (95% confidence level based on the Wilcoxon Rank Test (WRT)) from the long-term (2012-2018) seasonal average. The "Sig Pixel %" label indicates the number of pixels in the domain with significant differences.



733

734 **Figure 3:** SC0₃ (DU) from GOME-2 over Europe for May to August in (left column) 2017, (centre
 735 column) 2018 and (right column) 2018-2017 difference.

736

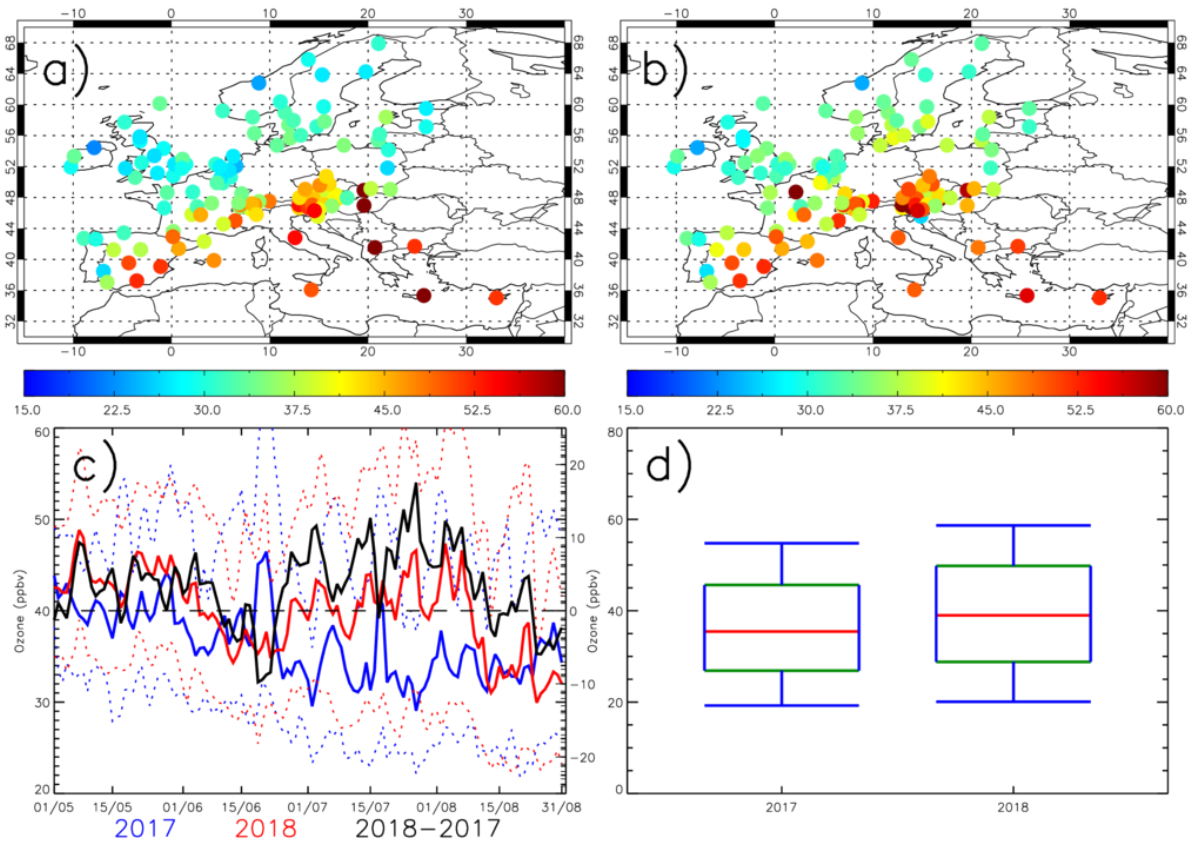


737

738 **Figure 4:** SCO₃ (DU) for May to August in 2017 (left column), 2018 (centre column) and 2018-2017
 739 difference (right column) over Europe retrieved from MetOp-A IASI, MHS and AMSU by the IMS
 740 scheme.

741

742



743

744

745

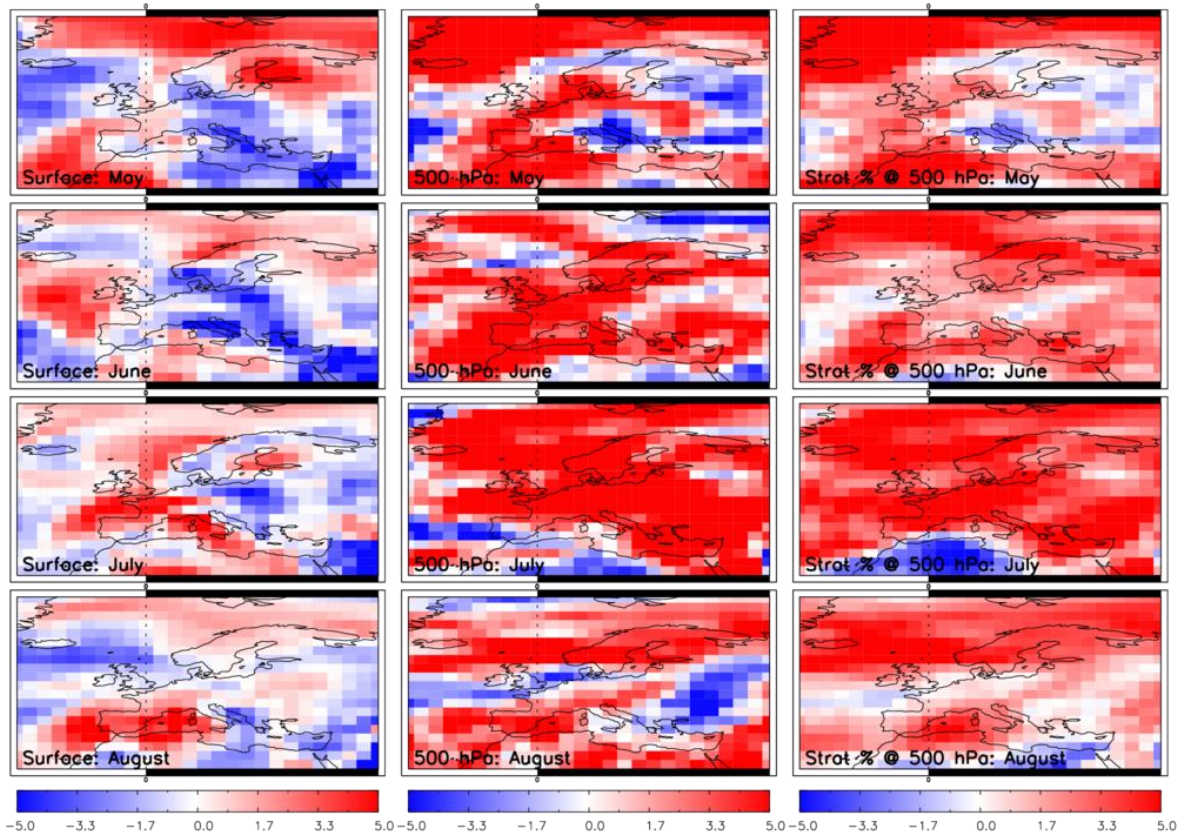
746

747

748

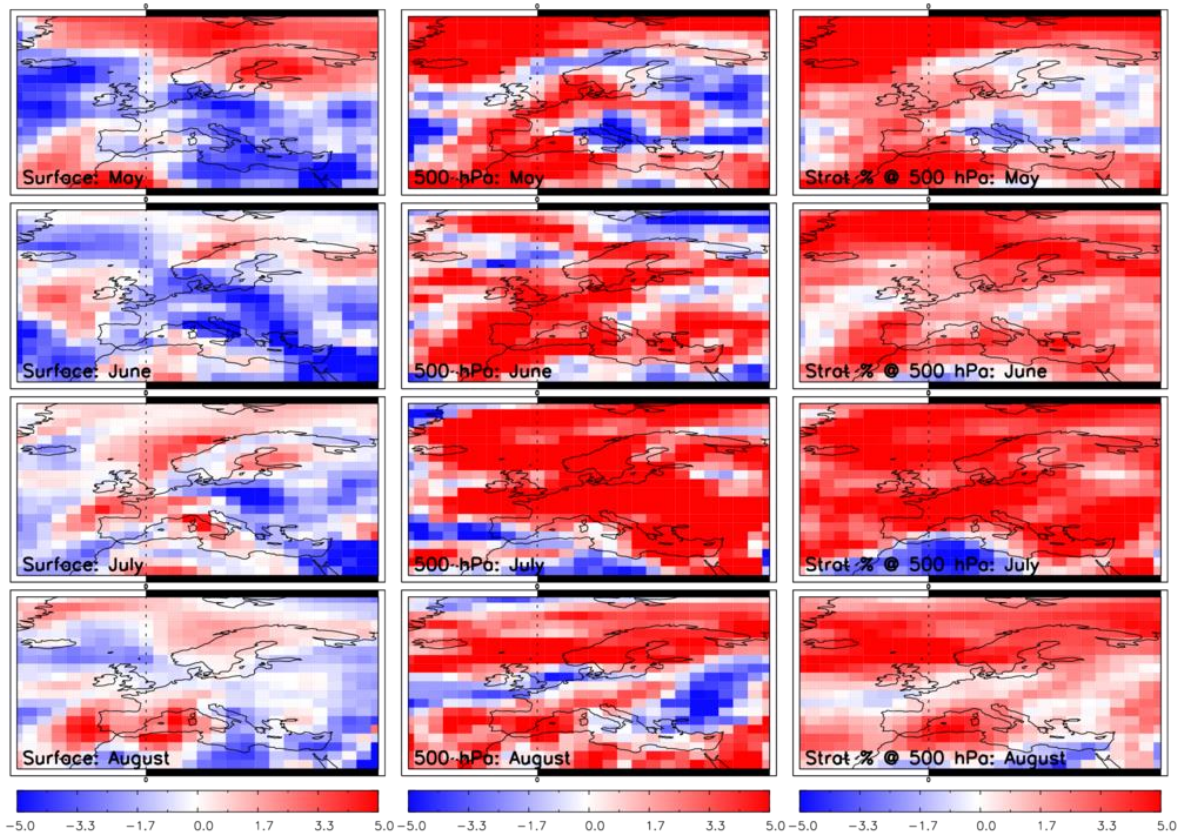
749

Figure 5: European surface ozone (ppbv) for a) May-June-July-August (MJJA) 2017, b) MJJA 2018), c) regional mean time series (dotted lines show mean \pm standard deviation) for MJJA 2017 (blue), MJJA 2018 (red) and the 2018-2017 difference (black) and d) box-whisker plots for MJJA 2017 and 2018. In panel d) the median, 25th & 75th percentiles and 10th & 90th percentiles are shown by the red, green and blue lines, respectively.



750
 751
 752
 753
 754

Figure 6: TOMCAT ozone (ppbv) 2018-2017 differences for May to August for the surface (left column), 500 hPa (centre column) and the stratospheric contribution (%) to the 500 hPa layer (right column).



755

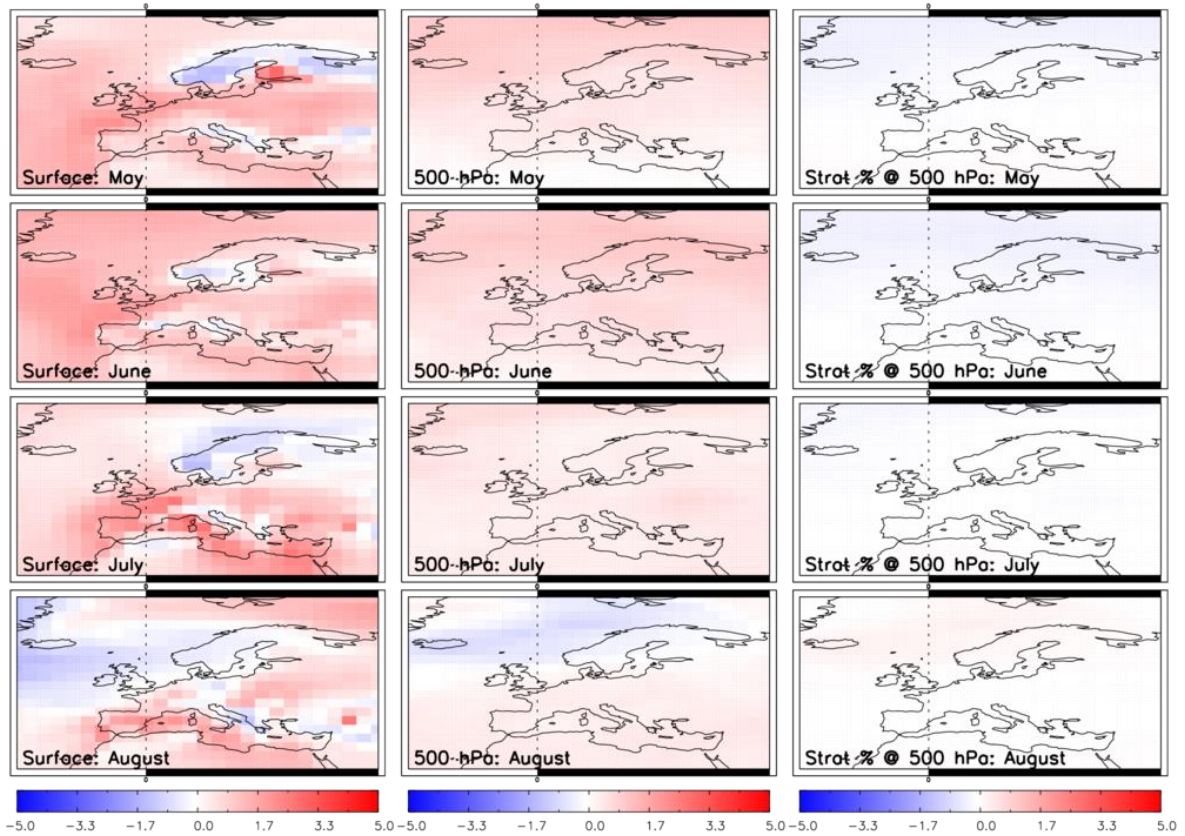
756

757

758

759

Figure 7: TOMCAT ozone (ppbv) 2018-2017 differences for May to August for the fixed emissions simulation (Fixed_EMIS) for the surface (left column), 500 hPa (centre column) and the stratospheric contribution (%) to the 500 hPa layer (right column).



760

761

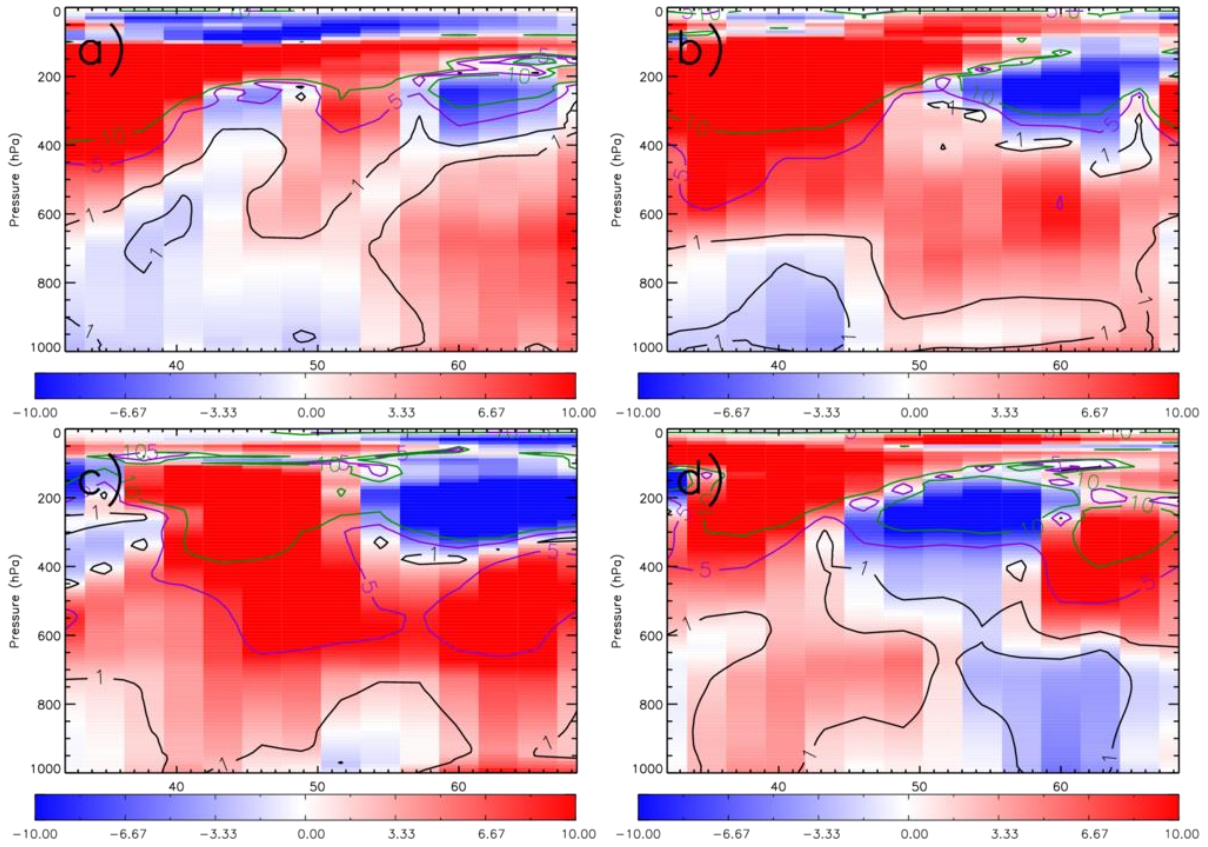
Figure 8: TOMCAT ozone (ppbv) 2018-2017 differences for May to August for the fixed meteorology simulation (Fixed_MET) for the surface (left column), 500 hPa (centre column) and the stratospheric contribution (%) to the 500 hPa layer (right column).

764

765

766

767



768

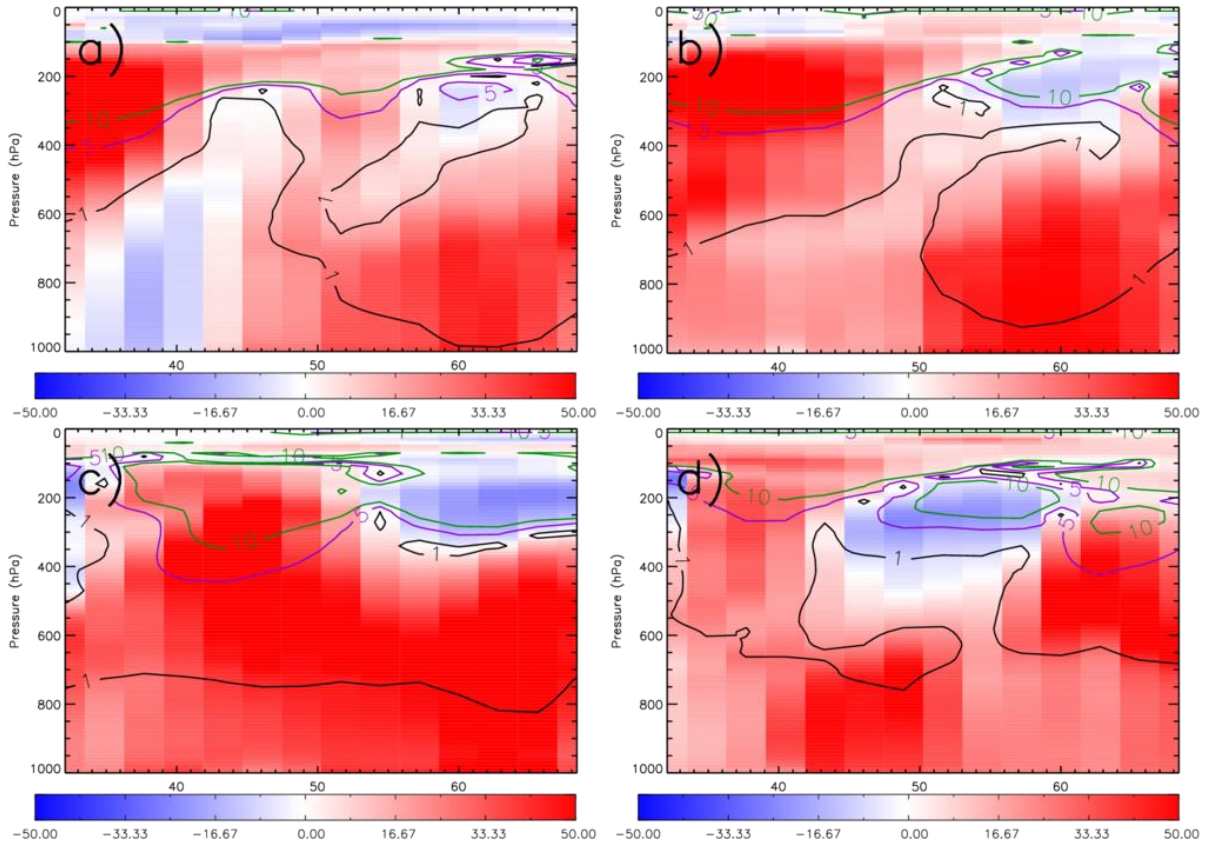
769

770

771

772

Figure 9: TOMCAT ozone, zonally averaged between 20°W and 40°E, 2018-2017 percentage differences (absolute difference (ppbv) shown as solid lines) from the control simulation. Panels a)-d) represent the monthly averages for May, June, July and August.



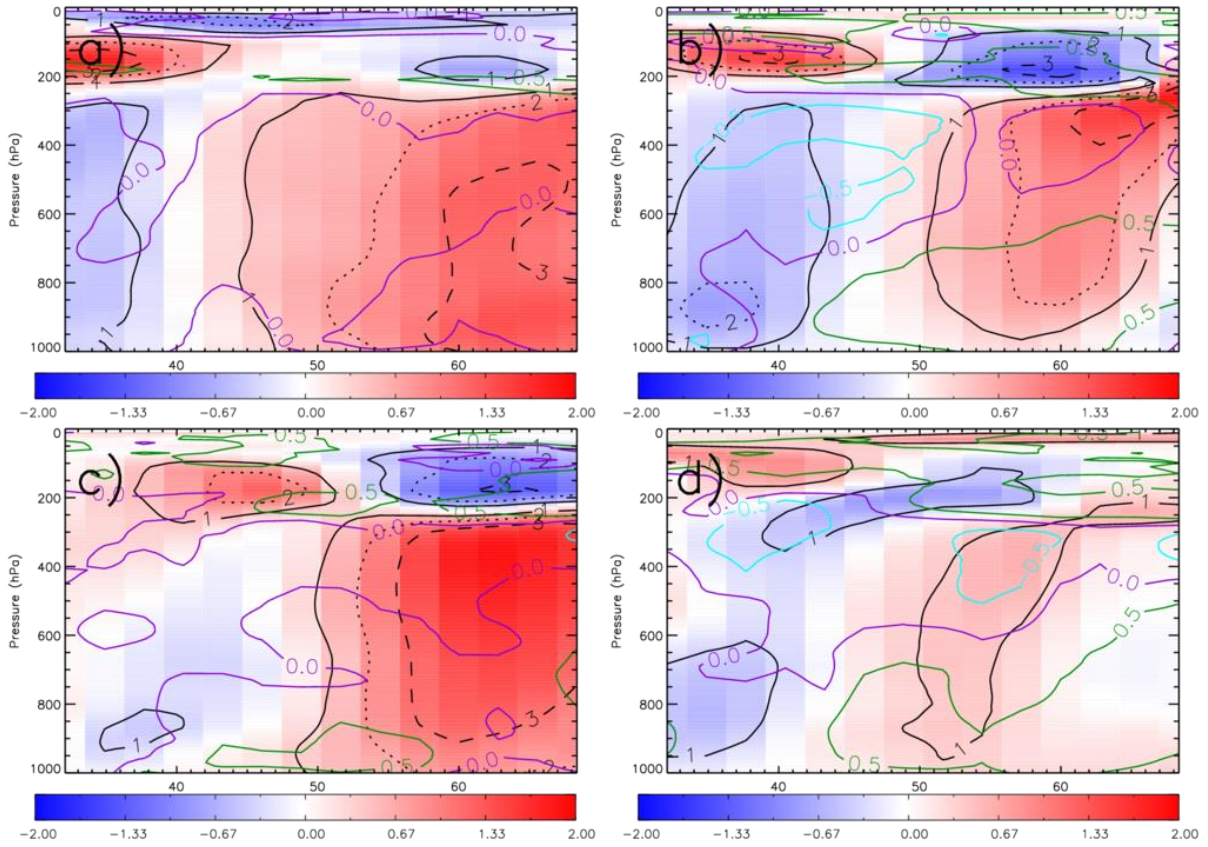
773

774 **Figure 10:** TOMCAT stratospheric ozone tracer, zonally averaged between 20°W and 40°E, 2018-2017
 775 percentage differences (absolute difference (ppbv) shown as solid lines) from the control simulation.
 776 Panels a)-d) represent the monthly averages for May, June, July and August.

777

778

779



780

781 **Figure 11:** TOMCAT temperature, zonally averaged between 20°W and 40°E, 2018-2017 percentage
 782 differences (absolute difference (K) shown by black solid, dotted and dashed lines) from the control
 783 simulation. Overplotted are contours of the temporal correlation (i.e. within each grid box) between
 784 the temperature and ozone 2018-2017 differences. Panels a)-d) represent the monthly averages for
 785 May, June, July and August.

786

787

788

789

790

791

792

793

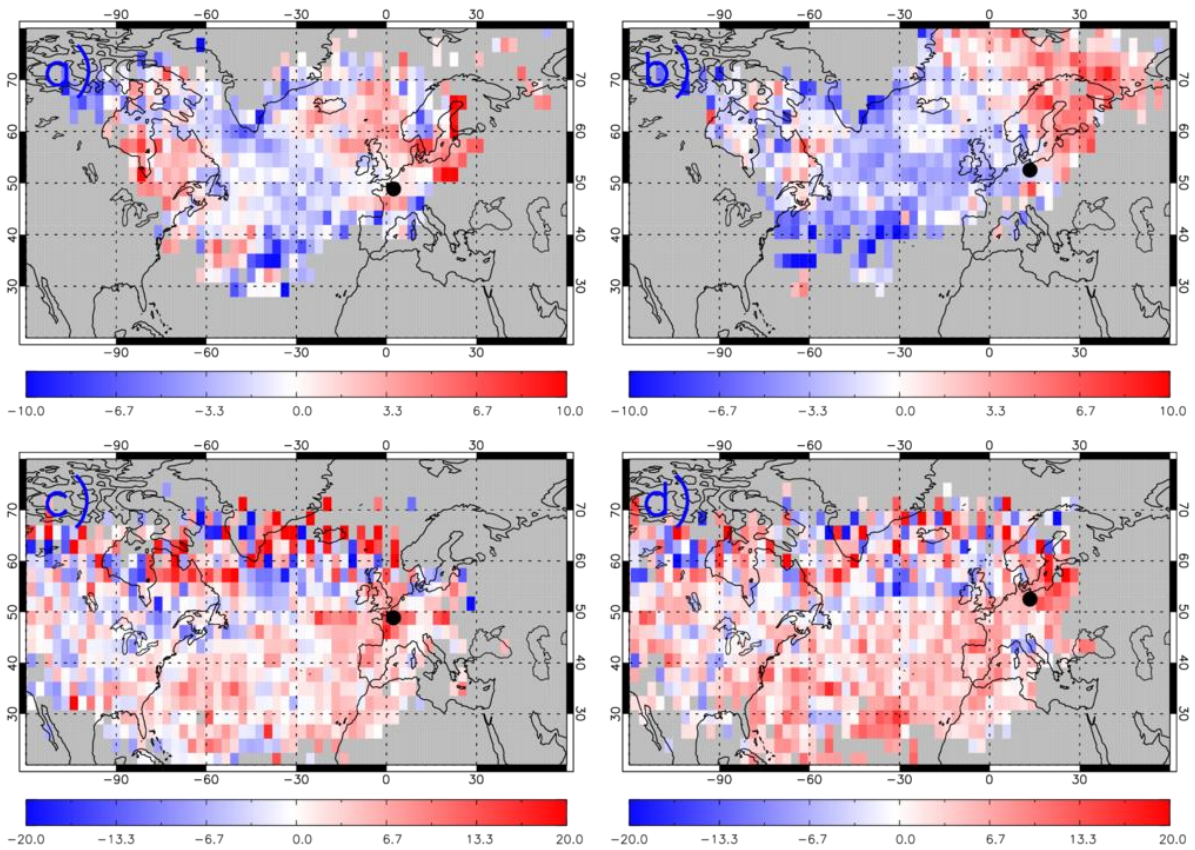
794

795

796

797

798



800

801 **Figure 12:** The difference between May-August 2018 and May-August 2017 (i.e. 2018-2017) ROTRAJ
 802 back-trajectories (10 days), weighted by the average TOMCAT O_3 (ppbv) concentration along each
 803 trajectory path, gridded onto the TOMCAT horizontal resolution for a) Paris at the surface, b) Berlin
 804 at the surface, c) Paris at approximately 500 hPa and d) Berlin at approximately 500 hPa. The black
 805 circles represent the location of Paris or Berlin, where the trajectories were released from.

806